iScience

CellPress
OPEN ACCESS

Article

Long non-coding RNA *LHX1-DT* regulates cardiomyocyte differentiation through H2A.Z-mediated LHX1 transcriptional activation

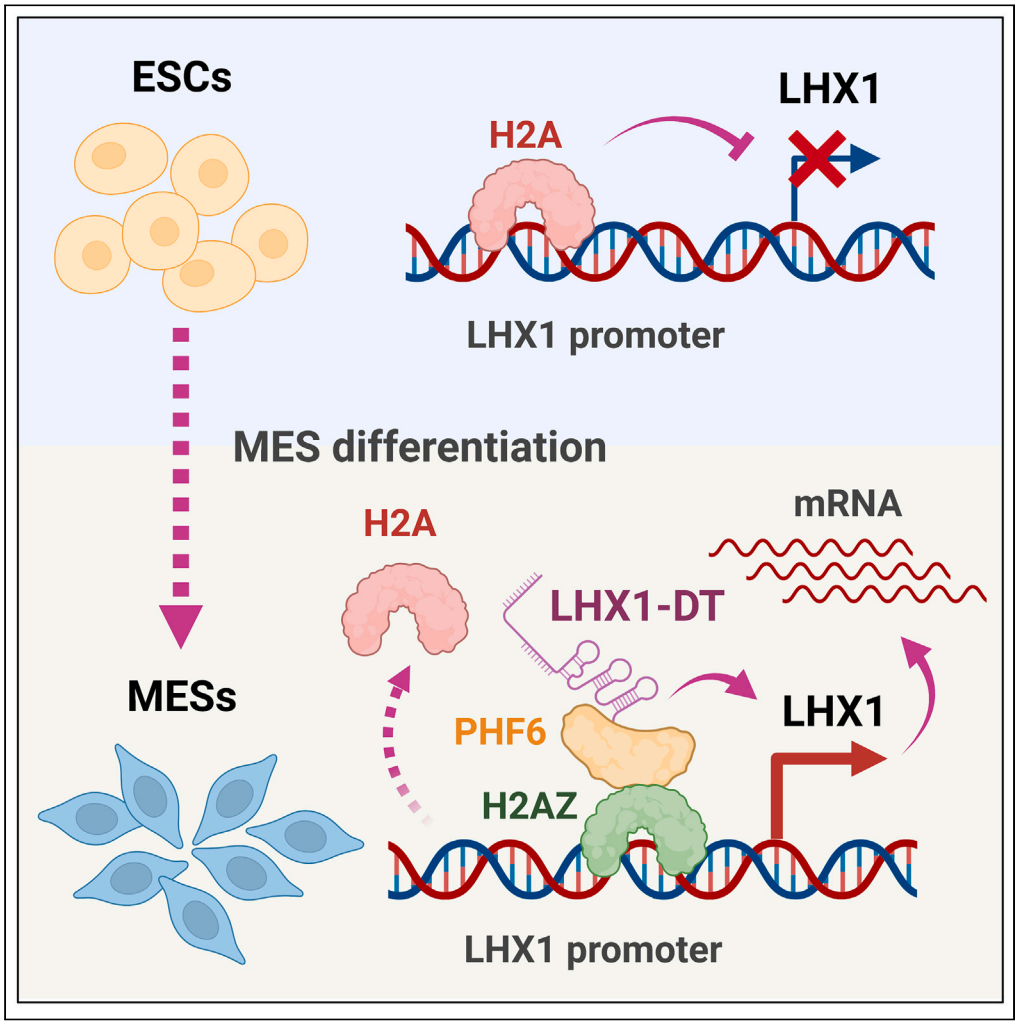

Qi Yu, Benzhi Cai, Yong Zhang, ..., Haodi Wu, Baofeng Yang, Ying Zhang

haodi@pitt.edu (H.W.)
yangbf@ems.hrbmu.edu.cn (B.Y.)
jennying223@126.com (Y.Z.)

Highlights

LHX1-DT plays a regulatory role in cardiac differentiation

LHX1-DT acts as an upstream regulator of LHX1 during mesoderm stage

LHX1-DT modulates the exchange of H2A.Z with H2A at the LHX1 promoter through its interaction with PHF6

Yu et al., iScience *26*, 108051
November 17, 2023 © 2023 The Authors.
https://doi.org/10.1016/j.isci.2023.108051

iScience

CellPress
OPEN ACCESS

Article

Long non-coding RNA *LHX1-DT* regulates cardiomyocyte differentiation through H2A.Z-mediated LHX1 transcriptional activation

Qi Yu,[1,2,7] Benzhi Cai,[1,3,7] Yong Zhang,[1,7] Juan Xu,[4] Dongping Liu,[1] Xiyang Zhang,[1] Zhenbo Han,[5] Yingying Ma,[4] Lei Jiao,[1] Manyu Gong,[1] Xuewen Yang,[1] Yanying Wang,[1] Haodong Li,[1] Lihua Sun,[1] Yu Bian,[1] Fan Yang,[1] Lina Xuan,[1] Haodi Wu,[2,*] Baofeng Yang,[1,6,*] and Ying Zhang[1,8,*]

SUMMARY

Long non-coding RNAs (lncRNAs) play widespread roles in various processes. However, there is still limited understanding of the precise mechanisms through which they regulate early stage cardiomyocyte differentiation. In this study, we identified a specific lncRNA called *LHX1-DT*, which is transcribed from a bidirectional promoter of LIM Homeobox 1 (LHX1) gene. Our findings demonstrated that *LHX1-DT* is nuclear-localized and transiently elevated expression along with LHX1 during early differentiation of cardiomyocytes. The phenotype was rescued by overexpression of LHX1 into the *LHX1-DT*$^{-/-}$ hESCs, indicating LHX1 is the downstream of *LHX1-DT*. Mechanistically, we discovered that *LHX1-DT* physically interacted with RNA/histone-binding protein PHF6 during mesoderm commitment and efficiently replaced conventional histone H2A with a histone variant H2A.Z at the promoter region of LHX1. In summary, our work uncovers a novel lncRNA, *LHX1-DT*, which plays a vital role in mediating the exchange of histone variants H2A.Z and H2A at the promoter region of LHX1.

INTRODUCTION

Cardiovascular disease is one of the leading causes of human death globally.[1] Cardiomyocytes are considered terminally differentiated cells, which exhibit limited proliferative and regenerative capabilities once they are damaged or injured. This characteristic renders the loss of cardiomyocytes generally irreversible, posing a significant challenge in the field of cardiac medicine; it is therefore highly desirable to develop new approaches for circumventing the problem.[2] Recent studies have proved that hESC-derived cardiomyocytes can restore the function of infarcted hearts in non-human primate models.[3] Nevertheless, the effectiveness and safety of cell therapy are still limited due to many challenges, such as immature excitation-contraction, proarrhythmic risk, and lack of sufficient cardiomyocytes. Thus, illuminating the underlying mechanisms for the early events of human cardiogenesis holds the key to resolving these issues. The heart is the first functional organ to be formed during vertebrate embryogenesis. In mammals, all organs are derived from three primary germ layers including endoderm, mesoderm, and ectoderm.[4] Cardiogenesis is a stepwise process involving the sequential differentiation from pluripotent stem cells to mesoderm, cardiac progenitor cells, and ultimately cardiomyocytes.[5] Human pluripotent stem cells, encompassing human embryonic stem cells (hESCs) and human induced pluripotent stem cells (hiPSCs), offer an opportunity to recapitulate the developmental process within embryos and also serve as a novel valuable research platform for improving the understanding of cell-fate specification and studying drug cardiotoxicity.[6,7]

Cardiac differentiation process depends on a precise temporal control of gene expression patterns. Disruption of this regulatory mechanism can give rise to congenital heart diseases.[8] Thus, it is crucial to unravel the transcriptional networks and molecular switches governing cardiac commitment, enabling a deeper understanding of the early stage cardiogenesis and discover novel therapeutic targets or approaches for treating cardiac diseases. However, the regulatory mechanisms orchestrating the coordination of embryonic developmental transitions remain poorly understood.

[1]Department of Pharmacology (State-Province Key Laboratories of Biomedicine-Pharmaceutics of China, Key Laboratory of Cardiovascular Medicine Research, Ministry of Education), College of Pharmacy, Harbin Medical University, Harbin, Heilongjiang 150081, China
[2]Heart, Lung, and Blood Vascular Medicine Institute, Division of Cardiology, Department of Medicine, University of Pittsburgh School of Medicine, Pittsburgh, PA 15261, USA
[3]Department of Pharmacy at The Second Affiliated Hospital, and Department of Pharmacology at College of Pharmacy (The Key Laboratory of Cardiovascular Medicine Research, Ministry of Education), Harbin Medical University, Harbin 150081, China
[4]College of Bioinformatics Science and Technology, Harbin Medical University, Harbin, Heilongjiang 150081, China
[5]Department of Pharmacology & Regenerative Medicine, The University of Illinois College of Medicine, 909 S Wolcott Avenue, COMRB 4100, Chicago, IL 60612, USA
[6]Research Unit of Noninfectious Chronic Diseases in Frigid Zone, Chinese Academy of Medical Sciences (2019RU070), Harbin 150086, China
[7]These authors contributed equally
[8]Lead contact
*Correspondence: haodi@pitt.edu (H.W.), yangbf@ems.hrbmu.edu.cn (B.Y.), jennying223@126.com (Y.Z.)
https://doi.org/10.1016/j.isci.2023.108051

This is an open access article under the CC BY-NC-ND license (http://creativecommons.org/licenses/by-nc-nd/4.0/).

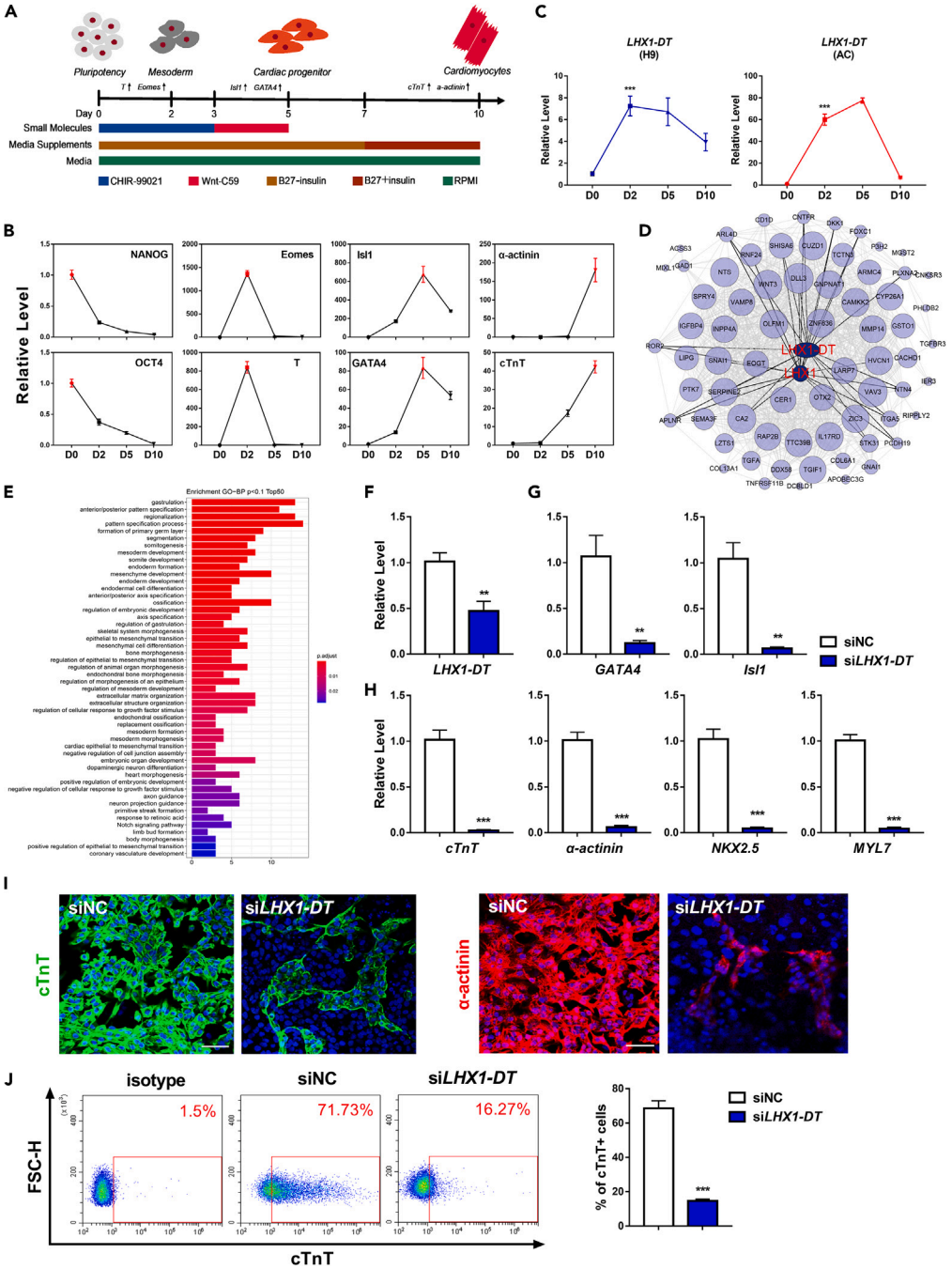

Figure 1. Identification of candidate lncRNAs during the early stage of cardiomyocyte differentiation

(A) The schema of cardiomyocyte differentiation protocol from human PSCs.

(B and C) qRT-PCR analysis of gene expression in all cells at the corresponding time points such as Day 0 (pluripotency genes: NANOG and OCT4), Day 2 (mesoderm genes: Eomes and T), Day 5 (cardiac progenitor markers: Isl1 and GATA4), and Day10 (cardiomyocytes: α-actinin and cTnT), n = 4 (C) qRT-PCR analysis of *LHX1-DT* expression on the indicated days of cardiac differentiation from hESC line (H9) and hiPSC line (AC). ***$p < 0.001$, n = 4.

(D) *LHX1-DT*-mRNA co-expression network analysis by Pearson's correlation. The network of *LHX1-DT* and mRNA were generated using Pearson's correlation coefficient ≥ 0.6, and FDR <0.1.

(E) Enriched GO terms of protein-coding genes that linked to the lncRNA co-expressed during cardiac differentiation.

(F) qRT-PCR analysis of *LHX1-DT* expression in H9 on Day 2 after *LHX1-DT* silencing. **$p < 0.01$, n = 4.

CellPress
OPEN ACCESS

Figure 1. *Continued*

(G and H) qRT-PCR analysis of the expression level of cardiac progenitor markers (GATA4 and Isl1) on Day 5 and cardiomyocyte markers (cTnT, α-actinin, NKX2.5, MYL7) on Day 10 in *LHX1-DT* depleted hESCs. **$p < 0.01$, ***$p < 0.001$, n = 4.

(I) Immunostaining of cTnT (green) and α-actinin (red) in siNC and *LHX1-DT* silencing cells on Day 10 of CM differentiation. Scale bar, 50 μm, n = 4.

(J) Representative flow cytometry analysis of the percentage of cTnT-positive cells between si*LHX1-DT* and siNC cells. ***$p < 0.001$, n = 4. Data are presented as mean ± SEM.

Long non-coding RNAs (lncRNAs) are widely defined as transcripts over 200 nucleotides in length and existing limited protein-coding activity.[9] Despite over 77,900 lncRNAs have been identified in RefLnc database, the functions of many lncRNAs remain elusive, partly due to the species specificity.[10,11] Over the past decade, numerous studies have found that lncRNAs can be functionally divided into signal lncRNAs, decoy lncRNAs, guide lncRNAs, scaffold lncRNAs, and enhancer lncRNAs, which regulate gene expression through diverse mechanisms.[12–16] LncRNAs play essential roles in various cellular processes in the context of lineage commitment, especially in cardiac lineage commitment.[17,18] For instance, Bvht acts as an upstream factor of Mesp1 by interacting with Suz12 to activate the core cardiovascular gene network.[19] Linc1405 facilitates the binding of the Eomes/WDR5/GCN5 complex to the enhancer region of Mesp1 gene and activates its expression during cardiac mesoderm specification in embryonic stem cells.[20] Despite these seminal findings about cardiac-related lncRNAs, the regulatory mechanism of lncRNAs in cardiac lineage commitment is still unclear.

In this study, we identified a unique lncRNA, termed LHX1 divergent transcript (*LHX1-DT*), which exerts regulatory effects on cardiac lineage differentiation. LIM homeobox 1 (LHX1), a transcription factor characterized by a homeodomain DNA-binding region and two Cys-rich LIM domains, mediates protein-protein interactions.[21] LHX1 is critical for cardiac differentiation at mesoendodermal stage and head development in mouse models.[22,23] *LHX1-DT*, a divergent lncRNA transcribed in the opposite direction to a sense protein-coding gene LHX1, possesses the potential to affect the transcription of neighboring genes. Here, we dissected the expression patterns of LHX1 and *LHX1-DT* during cardiomyocyte differentiation. Subsequently, we investigated the biological link and the differential regulatory mechanisms between LHX1 and *LHX1-DT*.

RESULTS

Identification of candidate lncRNAs during the early stage of cardiomyocyte differentiation

LncRNAs have been shown to play prominent roles in lineage-specific differentiation processes of human pluripotent stem cells.[24,25] We focused on the role of *LHX1-DT*, which is transcribed close to the mesoendoderm gene LHX1. We first employed a monolayer-differentiation method to generate cardiomyocytes from two different cell lines: the hESC line H9 and the hiPSC line AC[26] (Figure 1A). The population of cardiomyocytes was 70% after the initial confluency of H9 and AC lines for differentiation reached 80–90% and 80–85%, respectively.

In this study, we used 4 populations isolated at different time points during the differentiation process, including Day 0 (Pluripotent stem cell, PSC), Day 2 (Mesoderm, MES), Day 5 (Cardiac progenitor, CP), and Day10 (Cardiomyocyte, CM). Cell morphological alterations at different differentiation stages were monitored and recorded by light microscopy (Figure S1A). To validate the effectiveness of the monolayer-differentiation method for studying cardiomyocyte differentiation, the expression levels of specific marker genes were analyzed at each time point using quantitative real-time PCR (qRT-PCR). The marker genes included pluripotency genes NANOG and OCT4 (Day 0), mesoderm marker genes Eomes and T (Day2), cardiac progenitor marker genes Isl1 and GATA4 (Day5), and cardiac-specific genes α-actinin and cTnT (Day10). As expected, these marker genes exhibited characteristic high-expression levels at their respective differentiation stages, confirming the successful differentiation of cardiomyocytes using the monolayer-differentiation method (Figure 1B).

Then we performed qRT-PCR verification on the candidate lncRNAs identified from our previous global survey of ncRNA transcriptome profiles in PSC, MES, CP, and CM during cardiac differentiation.[27] In coincidence with the transcriptome profiles, the expression level of *RP11-445F12.1* (*LHX1-DT*), along with several other lncRNAs including *LINC00467*, *RP3-428L16.2*, *RP11-829H16.3*, and *RP11-445F12.2* increased in MES and *LINC01021*, *MEIS1-AS2*, *AC009518.4*, *LINC01356*, and *LINC01198* were upregulated in CP of cardiac differentiation (Figure S1B). *LHX1-DT* has no apparent protein-coding potential according to the analyses by coding potential assessment tool (CPAT),[28] coding potential calculator 2 (CPC2),[29] and PhyloCSF[30] (Figures S2A–S2C). Moreover, we observed a marked increase of *LHX1-DT* expression during cardiac mesoderm specification in both H9 and AC cell lines (Figure 1C).

The transcriptomic analyses on the human cardiac differentiation in RUES2 hESC lines uncovered that *LHX1-DT* was highly expressed specifically at the mesoderm stage compared to the other three stages. Co-expression analysis identified 16 mRNAs specifically expressed at the mesoderm stage that were connected to *LHX1-DT*, forming a closely connected network (Figure 1D). As expected, the protein-coding genes (PCG) were mainly associated with early differentiation such as gastrulation, posterior pattern specification, and mesoderm development (Figure 1E).

A question we asked was whether the upregulation of *LHX1-DT* during the mesoderm stage is a contributor to cardiac differentiation. To answer this question, we employed a loss-of-function approach using siRNAs targeting human *LHX1-DT* and investigated if silencing *LHX1-DT* would block cardiac differentiation in hESCs. Significant knock down of *LHX1-DT* was observed after transfection of siRNA but not of the scrambled siRNA (siNC, Figure 1F). As illustrated in Figure 1G, *LHX1-DT* knockdown decreased the expression of cardiac progenitor marker genes GATA4 and Isl1 on Day 5. In addition, the transfection of *LHX1-DT* siRNA significantly decreased the expression of cardiomyocyte marker genes cTnT and α-actinin, suggesting an inhibition of cardiomyocyte differentiation (Figure 1H). The earliest marker for cardiogenic cells NKX2.5 and functional cardiomyocyte-specific marker MYL7 were also downregulated following *LHX1-DT* silence on Day 10 (Figure 1H).

The expression of cardiac-specific myofilament protein cTnT and sarcomeric α-actinin decreased in *LHX1-DT*-depleted hESCs as assessed by immunofluorescence analysis (Figure 1I). In addition, a lower ratio of cardiac troponin T ($cTnT^+$) CMs was observed in the *LHX1-DT* siRNA group compared to the siNC group (Figure 1J).

LHX1-DT regulates a core network of genes to drive cardiac differentiation

The aforementioned results suggest that *LHX1-DT* exhibits abundant expression at the mesoderm stage and plays a crucial role in promoting cardiac differentiation. To further investigate the downstream targets of *LHX1-DT* in mesoderm differentiation on Day 2, we employed RNA-seq to analyze cells with silenced *LHX1-DT* expression, as well as cells treated with siNC for comparison.

We identified 2,338 genes (Benjamini and Hochberg (BH) adjusted p-value <0.05, fold change (FC) > 1.5 or FC < 0.67) that displayed significant differential expression in *LHX1-DT*-depleted cells compared to siNC-treated cells. Following the knock down of *LHX1-DT*, a total of 873 genes exhibited an upregulation in expression, while 1,465 genes displayed a downregulation. Notably, among the downregulated genes, several important mesodermal markers, including Eomes, T, Mesp1, and LHX1 were identified. (Figure 2A). Principal component analysis (PCA) of the transcriptomic data showed that gene expression profiles in *LHX1-DT*-silenced cells differed from those observed in siNC cells (Figure 2B). Furthermore, gene ontology (GO) term analysis showed that the differentially expressed genes were associated with protein binding and biological processes related to regulation of cellular process, developmental process, and cell differentiation (Figure 2C). Additionally, the Kyoto encyclopedia of genes and genomes (KEGG) pathway enrichment analysis indicated that the downregulated genes primarily participate in ESC differentiation pathways such as the PI3K-Akt signaling pathway, the MAPK signaling pathway, and the Wnt signaling pathway (Figure 2D). Interestingly, gene set enrichment analysis (GSEA) unveiled that *LHX1-DT* silencing resulted in downregulation of genes associated with the mesendoderm (ME) while upregulating the expression of pluripotent genes on Day 2 (Figure 2E).

These results were further confirmed by qRT-PCR. *LHX1-DT* knockdown blocked the activation of mesoderm-related marker genes including Eomes, T, Mesp1, and LHX1 (Figure 2F). Moreover, the expression of ESC-specific genes such as SOX2, NANOG, and DNMT3B were maintained at high-expression levels in differentiated *LHX1-DT*-silenced cells (Figure 2G). Collectively, these findings strongly indicate that *LHX1-DT* serves as a crucial regulator of mesoderm differentiation.

Depletion of LHX1-DT does not affect pluripotency of hESCs

To explore the role of *LHX1-DT* in determining the fate of hESC, two *LHX1-DT*$^{-/-}$ hESC lines were generated from wild-type H9 hESCs (*LHX1-DT*$^{+/+}$) with CRISPR-Cas9 system as reported previously[31] (Figure 3A). The expression of *LHX1-DT* was confirmed to be significantly reduced in the two targeted hESC lines (*LHX1-DT*$^{-/-}$-1 and *LHX1-DT*$^{-/-}$-2) on Day 0 of cardiac differentiation (Figure 3B). In coincidence with the effects of *LHX1-DT* silencing, the levels of *LHX1-DT* and mesoderm-related marker genes were markedly decreased in *LHX1-DT*$^{-/-}$ hESC lines differentiated to Day 2, and cardiomyocyte-specific markers were downregulated as well in *LHX1-DT*$^{-/-}$ hESC lines differentiated to Day 10 (Figures 3C and 3D). These results indicated that *LHX1-DT*$^{-/-}$ hESC lines failed to differentiate into definitive mesoderm and cardiomyocyte. Moreover, knock down of *LHX1-DT* had no effect on colony morphology in *LHX1-DT*$^{+/+}$ cells (Figure 3E).

Another question that arose was whether *LHX1-DT* is involved in the maintenance of pluripotency in hESCs. The results obtained from qRT-PCR and immunostaining experiments, as illustrated in Figures 3F and 3G excluded this possibility: the mRNA and protein expression levels of pluripotency markers were comparable between *LHX1-DT*$^{-/-}$ and *LHX1-DT*$^{+/+}$ hESC lines, indicating that *LHX1-DT* does not play a significant role in maintaining pluripotency in hESCs.

LHX1-DT enhances LHX1 expression to promote cardiac differentiation

The results mentioned previously shed light on the role of *LHX1-DT* in mesoderm formation. However, it remained unclear the mechanism of *LHX1-DT* regulates cardiac lineage commitment of hESC. To address this question, we searched for the genomic context of *LHX1-DT* and its associated protein-coding genes. As shown in Figure 4A, *LHX1-DT* locates on the human chromosome 17q12 and transcribes from the nearby antisense strand of the promoter region of LHX1 gene, which is a master regulator of mesendoderm development.[32] They are highly conserved across the relationship between *LHX1-DT* and LHX1, we examined their expression patterns during cardiac differentiation. High expression of both *LHX1-DT* and LHX1 was observed at the mesoderm stage (Day 2) in RUES2 hESC lines (Figures S3A, S3B and 4B), additionally, high-chromatin accessibility was also observed based on the ATAC-seq data. More importantly, knock down of *LHX1-DT* led to a decreased expression of LHX1 during cardiac differentiation (Figures 2F and 3C), suggesting that *LHX1-DT* might regulate LHX1 expression during cardiac differentiation.

To further validate the findings from the bioinformatics analysis, we performed qRT-PCR to determine the time course of expression pattern of LHX1 and *LHX1-DT* during cardiac differentiation. The results depicted in Figure 4C clearly indicate that LHX1 exhibited an upregulation pattern similar to that of *LHX1-DT* during mesoderm differentiation. Furthermore, the co-localization of *LHX1-DT* and LHX1 in the nucleus of mesoderm-committed hESCs was also observed using fluorescent in situ hybridization (FISH) (Figure 4D).

The results prompted us to raise another question: whether LHX1 has a similar effect on cardiac differentiation like *LHX1-DT* does? To this end, we transfected siRNA against LHX1 into hESCs to silence LHX1 expression. We confirmed the efficiency of siLHX1 at the mesoderm stage through Western blot analysis and qRT-PCR (Figures 4E and 4F).

With loss of function approach, we found that knock down of LHX1 significantly increased the protein level of pluripotency marker OCT4 (Figure S4A) and decreased the expression of mesoderm markers T and Mesp1, but it had no influence on *LHX1-DT* expression on Day 2

CellPress
OPEN ACCESS

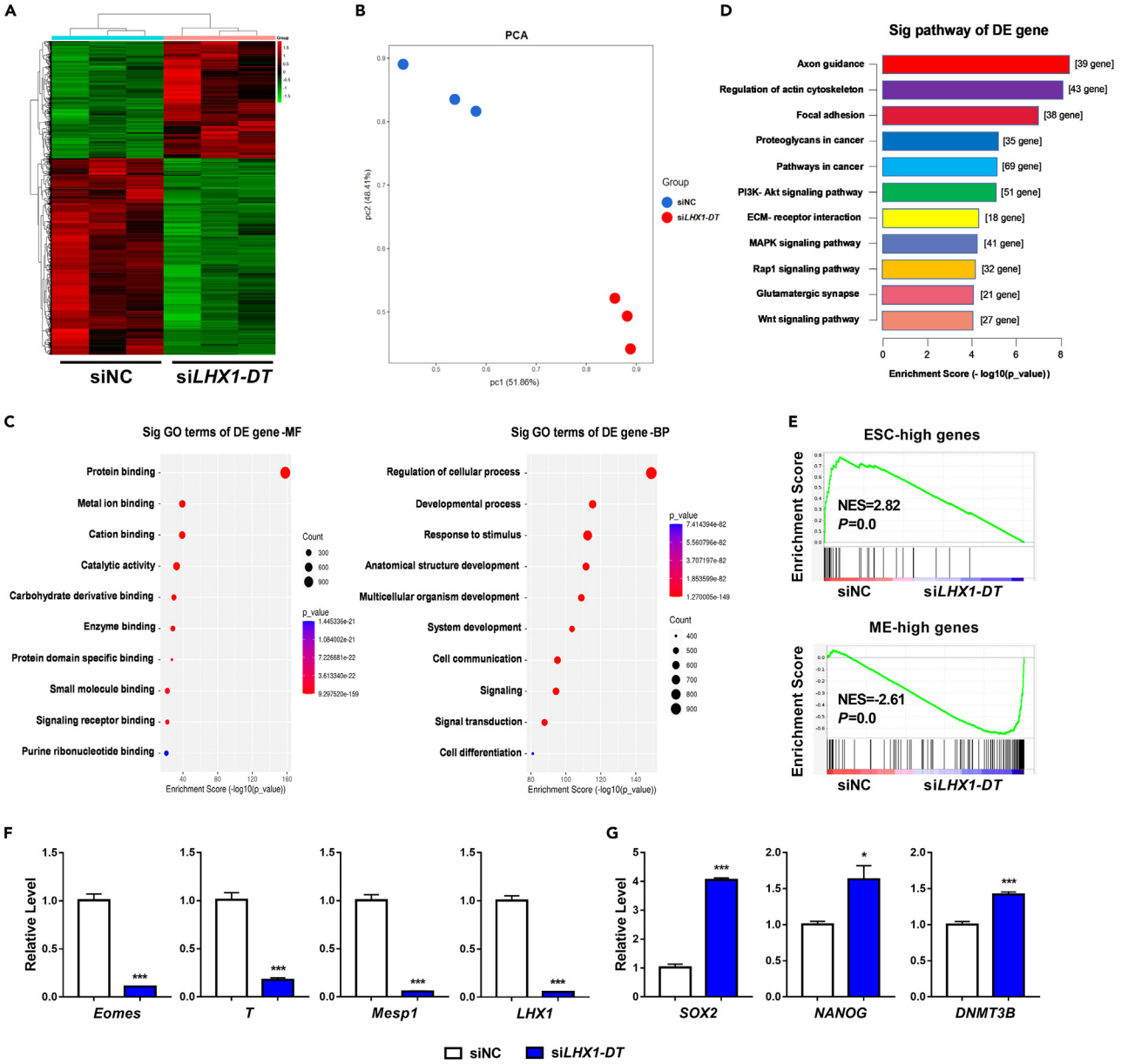

Figure 2. *LHX1-DT* regulates a core network of genes to drive cardiac differentiation

(A) Heatmap showing differential expressed genes (DEGs) between si*LHX1-DT* and siNC mesodermal cells on Day 2, n = 3.

(B) Principle component analysis (PCA) of DEGs revealed a clear separation between si*LHX1-DT* cells and siNC cells.

(C) Analysis of significant GO terms in DEGs between si*LHX1-DT* mesodermal cells and siNC mesodermal cells.

(D) KEGG pathway enrichment analysis for the DEGs in the *LHX1-DT* knockdown mesodermal cells.

(E) Gene set enrichment analysis (GSEA) of *LHX1-DT* knockdown cells versus siNC cells showing global downregulation of mesoderm genes and upregulation of pluripotent genes.

(F and G) qRT-PCR analysis of mesoderm marker genes (Eomes, T, Mesp1, and LHX1) and pluripotent marker genes (SOX2, NANOG, and DNMT3B) between si*LHX1-DT* and siNC on Day 2. *$p < 0.05$, ***$p < 0.001$, n = 4. Data are presented as mean ± SEM.

(Figure 4G). Moreover, knock down of LHX1 decreased the mRNA levels of cardiac progenitor markers GATA4 and Isl1, as well as cardiac-specific markers cTnT, α-actinin, NKX2.5, and MYL7 (Figure 4H and S4B). These results were further confirmed by immunofluorescence staining of cTnT and α-actinin as well (Figure 4I). In addition, the hESC-derived cardiomyocytes (hESC-CMs) were dissociated and analyzed by flow cytometry, a lower percentage of cTnT-positive cells was observed in the siLHX1 group (Figure 4J). These results indicated that LHX1 is required for proper cardiac differentiation.

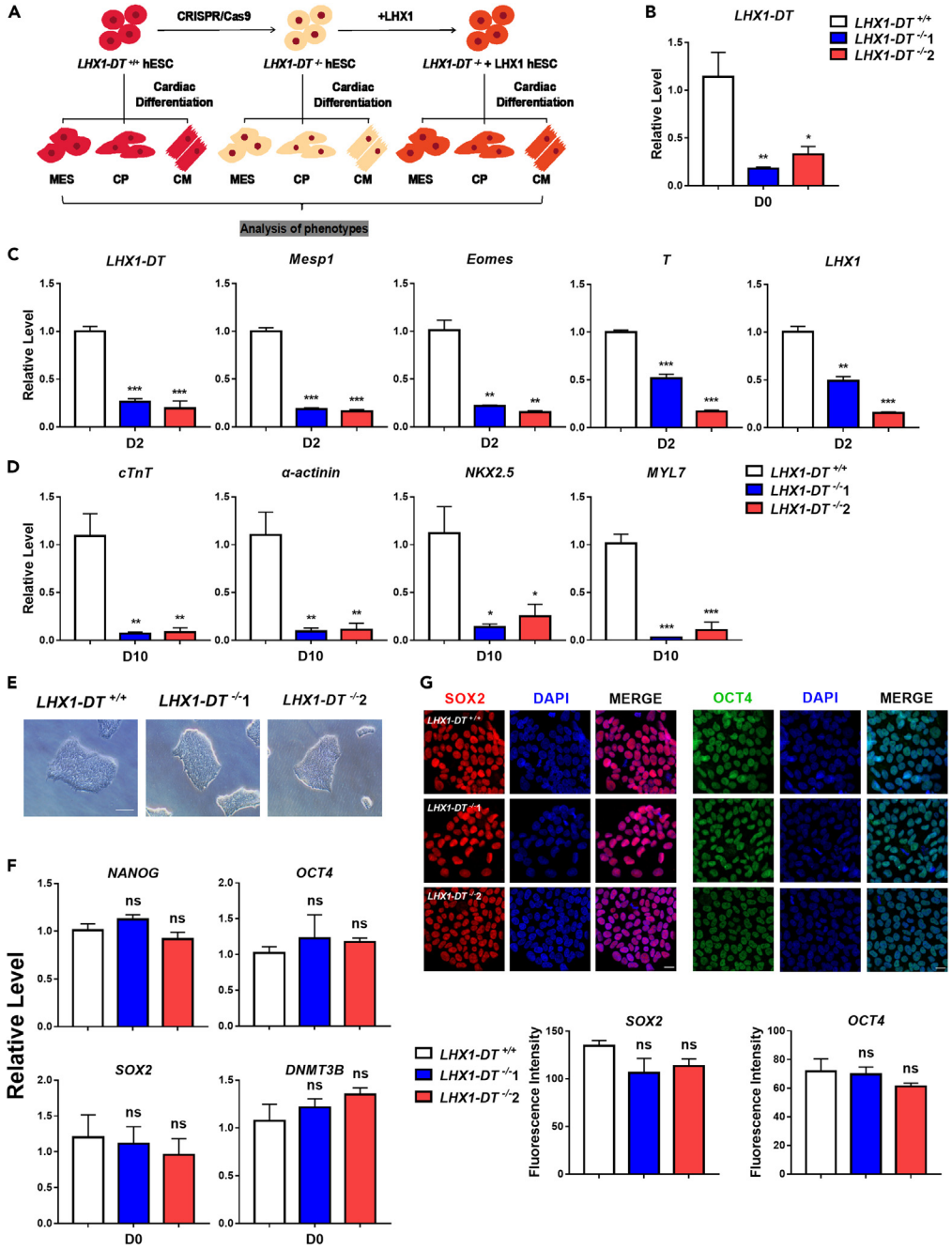

Figure 3. Depletion of *LHX1-DT* does not affect pluripotency of hESCs

(A) Schematic diagram of the generation of *LHX1-DT*$^{-/-}$ hESCs, illustrates the strategy for generating *LHX1-DT*$^{-/-}$ hESCs with CRISPR/Cas9 technology.

(B) qRT-PCR analysis of *LHX1-DT* expression in undifferentiated *LHX1-DT*$^{-/-}$ and *LHX1-DT*$^{+/+}$ hESCs. *p < 0.05, **p < 0.01, n = 6.

(C and D) qRT-PCR analysis of the expression of *LHX1-DT* and mesoderm markers (Mesp1, Eomes, T, and LHX1) on Day 2 and cardiomyocyte markers (cTnT, α-actinin, NKX2.5, MYL7) on Day 10 in *LHX1-DT* depleted hESCs. *p < 0.05, **p < 0.01, ***p < 0.001, n = 3–4.

(E) Microscope images for the morphology of *LHX1-DT*$^{-/-}$ and *LHX1-DT*$^{+/+}$ hESCs. Scale bars, 100 μm.

(F) qRT-PCR analysis of pluripotency markers NANOG, OCT4, SOX2, and DNMT3B in undifferentiated *LHX1-DT*$^{-/-}$ and *LHX1-DT*$^{+/+}$ hESCs, n = 6.

(G) Immunostaining of pluripotency markers SOX2 and OCT4 in the *LHX1-DT*$^{-/-}$ and *LHX1-DT*$^{+/+}$ hESCs. Scale bars, 20 μm.

Next, to investigate whether *LHX1-DT* regulates cardiac differentiation through LHX1-dependent, we introduced exogenous LHX1 into two *LHX1-DT*$^{-/-}$ hESC lines (Figure 3A). As expected, the introduction of exogenous LHX1 strongly rescued the expression of cardiac progenitor marker Isl1 on Day 5, as well as cardiac-specific genes including cTnT, α-actinin, NKX2.5, and MYL7 in the two *LHX1-DT*-silenced cell

CellPress
OPEN ACCESS

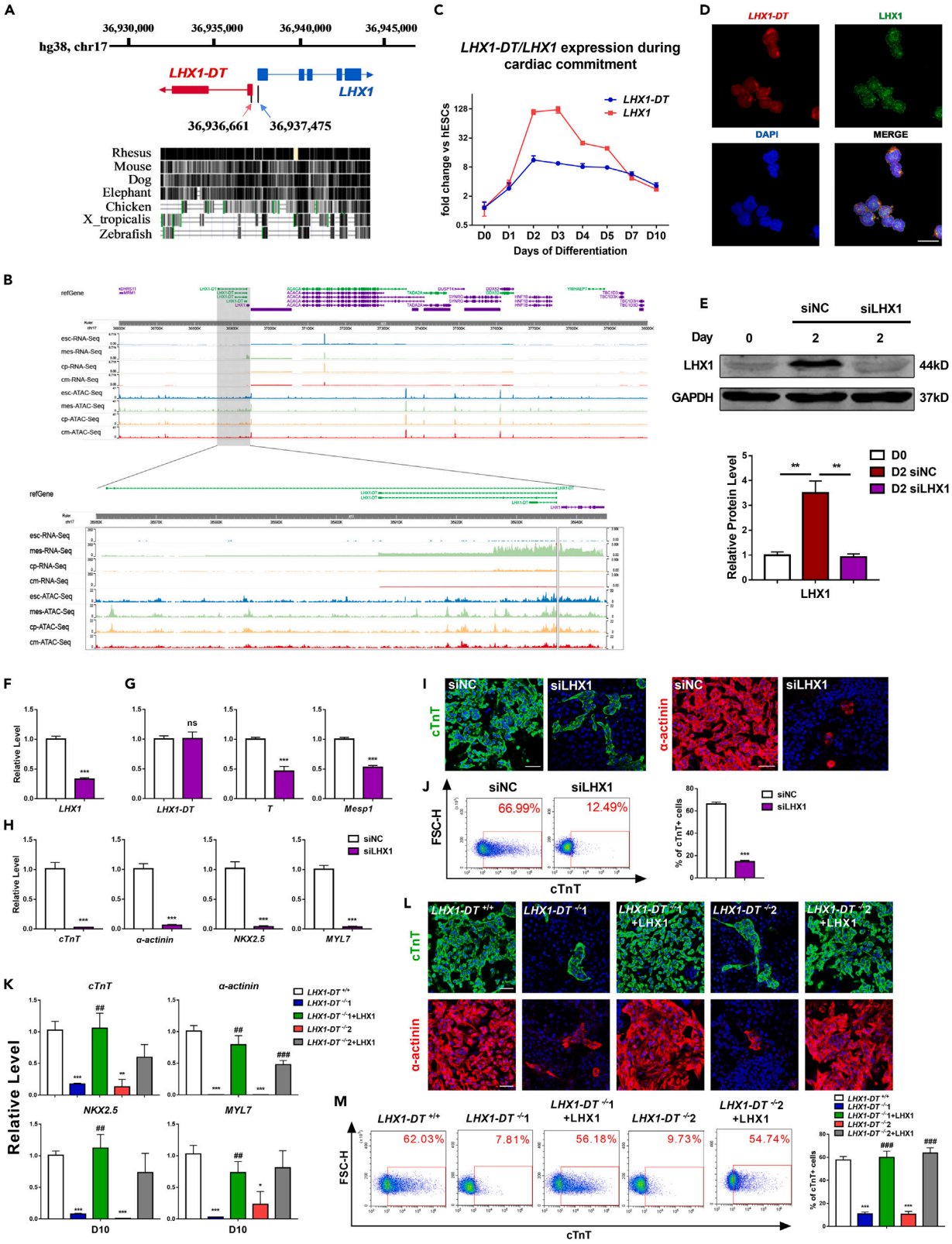

Figure 4. *LHX1-DT* enhances LHX1 expression to promote cardiac differentiation

(A) Schematic representation of the *LHX1-DT* and LHX1 gene locus and their sequence conservation analysis from UCSC genome browser. Red and blue arrows indicate the direction of transcription of *LHX1-DT* and LHX1 respectively.

(B) Genome browser track of the selected genomic regions around *LHX1-DT* and LHX1. The gray shadow rectangle showing the expression levels and ATAC signals of *LHX1-DT* and LHX1 at the four stages of cardiac development.

(C) qRT-PCR analysis of *LHX1-DT* and LHX1 expression during cardiac differentiation, n = 4.

(D) Localization of *LHX1-DT* and LHX1 in mesodermal cells derived from hESCs by FISH study. Scale bars, 20 μm, n = 4.

(E) Western blot analysis of LHX1 in undifferentiated and in mesoderm differentiating cells with *LHX1-DT* knockdown. $^{**}p < 0.01$, n = 3.

(F) qRT-PCR analysis of LHX1 expression in differentiating hESCs 2 days following siRNA transfection of cardiac differentiation. $^{***}p < 0.001$, n = 4.

(G and H) qRT-PCR analysis of the expression levels of *LHX1-DT* and mesoderm markers (T and Mesp1) on Day 2 and cardiomyocyte markers (cTnT, α-actinin, NKX2.5, and MYL7) on Day 10 in *LHX1-DT* depleted hESCs. $^{***}p < 0.001$, n = 4.

(I) Immunostaining of cTnT (green) and α-actinin (red) in LHX1 knockdown and siNC cells on Day 10 of CM differentiation. Scale bar, 50 μm, n = 4.

(J) Representative flow cytometry analysis of the percentage of cTnT-positive cardiomyocytes between siLHX1 and siNC group. $^{***}p < 0.001$, n = 3.

(K) qRT-PCR analysis of cardiac marker genes expression on Day 10 in *LHX1-DT*$^{+/+}$, *LHX1-DT*$^{-/-}$, and *LHX1-DT*$^{-/-}$ + LHX1 cells. $^{*}p < 0.05$, $^{**}p < 0.01$, $^{***}p < 0.001$ vs. *LHX1-DT*$^{+/+}$, n = 4. $^{\#\#}p < 0.01$, $^{\#\#\#}p < 0.001$ vs. *LHX1-DT*$^{-/-}$, n = 4.

(L) Immunostaining of cTnT (green) and α-actinin (red) in *LHX1-DT*$^{+/+}$, *LHX1-DT*$^{-/-}$, and *LHX1-DT*$^{-/-}$ + LHX1 cells on Day 10 of CM differentiation. Scale bar, 50 μm. Scale bars, 50 μm, n = 4.

(M) Representative flow cytometry analysis of the percentage of cTnT-positive cells in *LHX1-DT*$^{+/+}$, *LHX1-DT*$^{-/-}$, and *LHX1-DT*$^{-/-}$ + LHX1 cardiomyocytes. $^{***}p < 0.001$ vs. *LHX1-DT*$^{+/+}$, $^{\#\#\#}p < 0.001$ vs. *LHX1-DT*$^{-/-}$, n = 3. Data are presented as mean ± SEM.

lines on Day 10 (Figures S3C and 4K). These results were further confirmed by immunofluorescence staining of cTnT and α-actinin, as well as flow cytometry analysis of cTnT-positive cells (Figures 4L and 4M). Taken together, these results indicated that *LHX1-DT* promotes cardiac differentiation via LHX1.

Histone variant H2A.Z is incorporated into the promoter of LHX1 and promotes cardiomyocyte differentiation

The histone variant H2A.Z has been shown to facilitate licensing and activation during early mammalian development.[33,34] H2A.Z exhibits preferential occupancy on gene regulatory regions, such as promoter and enhancer, suggesting its important role in the regulation of gene transcription.[35–37] Further questions raised in our mind were whether H2A.Z can bind to the promoter region of LHX1 through protein-DNA interactions and whether such a binding is regulated by *LHX1-DT*. To shed light on these issues, we employed ChIP to investigate the direct binding between H2A.Z and the LHX1 promoter region. As illustrated in Figure 5A, the enrichment of H2A.Z protein at the promoter region of LHX1 was significantly increased during MES induction. Subsequently, we investigated the effects of H2A.Z on cardiomyocyte differentiation with loss-of-function strategy. We found that knock down of endogenous H2A.Z partially inhibited the protein levels of H2A.Z and LHX1 on Day 2 (Figure 5B). Moreover, the expression of H2A.Z mRNA exhibited similar changes to its protein levels on Day 2 (Figure 5C). Notably, we found that knock down of endogenous H2A.Z significantly decreased the expression of mesoderm markers, including LHX1, Eomes, T, and Mesp1, while increasing the expression of pluripotency markers NANOG and SOX2 on Day 2 (Figures 5D and S5A). Also, knock down of endogenous H2A.Z decreased the expression of cardiac progenitor markers GATA4 and Isl1 on Day 5 (Figure S5B), as well as the expression of cardiomyocyte markers, including cTnT, α-actinin, NKX2.5, and MYL7 on Day 10 (Figure 5E). Consistent with this differentiation failure, the mRNA levels of pluripotency marker genes SOX2 and NANOG were higher in H2A.Z knockdown cells (Figure 5F). Additionally, knock down of endogenous H2A.Z significantly decreased the proportion of cTnT^{+} cardiomyocytes detected by immunofluorescence (Figure 5G). Interestingly, we observed that knock down of *LHX1-DT*, LHX1, or H2A.Z disrupted the typical cellular morphology of cardiomyocytes and intercellular junctions (Figure S5C).

Considering that histone variants are generally assembled into nucleosomes by replacing their canonical counterpart.[38] Therefore, we assessed whether histone variant H2A.Z could efficiently replace conventional histone H2A at the LHX1 promoter region. As shown in Figure 5H, enrichment of H2A protein at the LHX1 promoter region was significantly decreased during mesoderm induction, which was in marked contrast to the enrichment of H2A.Z protein at the promoter region of LHX1. Taken together, these data demonstrate that H2A was replaced by H2A.Z at the promoter region of LHX1 during MES induction, and H2A.Z is required for the transcription for LHX1 in cardiac lineage commitment.

LHX1-DT promotes the replacement of H2A with H2A.Z on LHX1 promoter during mesoderm commitment

Although the aforementioned data have indicated that H2A was replaced by H2A.Z on the LHX1 promoter during mesoderm differentiation, it remained unclear whether *LHX1-DT* was involved in promoting this process. To shed light on this issue, we performed ChIP to detect the enrichment of H2A and H2A.Z at the promoter region of LHX1 at the mesoderm stage using si*LHX1-DT* to silence *LHX1-DT* expression. Our results demonstrated a robust reduction in H2A.Z enrichment and a significant increase in H2A enrichment at the LHX1 promoter region in the presence of si*LHX1-DT* (Figures 6A and 6B). Additionally, qRT-PCR analysis confirmed that knock down of H2A increased the expression of LHX1 and eomes on differentiation Day 2 (Figure S5D).

Next, we aimed to determine whether *LHX1-DT* acts upstream or downstream of the H2A.Z-LHX1 pathway. As illustrated in Figures 6C and 6D, the protein and mRNA levels (Figure 2F) of LHX1 were prominently decreased, while no significant alterations were observed in H2A.Z expression at both the protein and mRNA levels during the mesoderm stage upon silencing *LHX1-DT*. These results indicated that *LHX1-DT*

CellPress
OPEN ACCESS

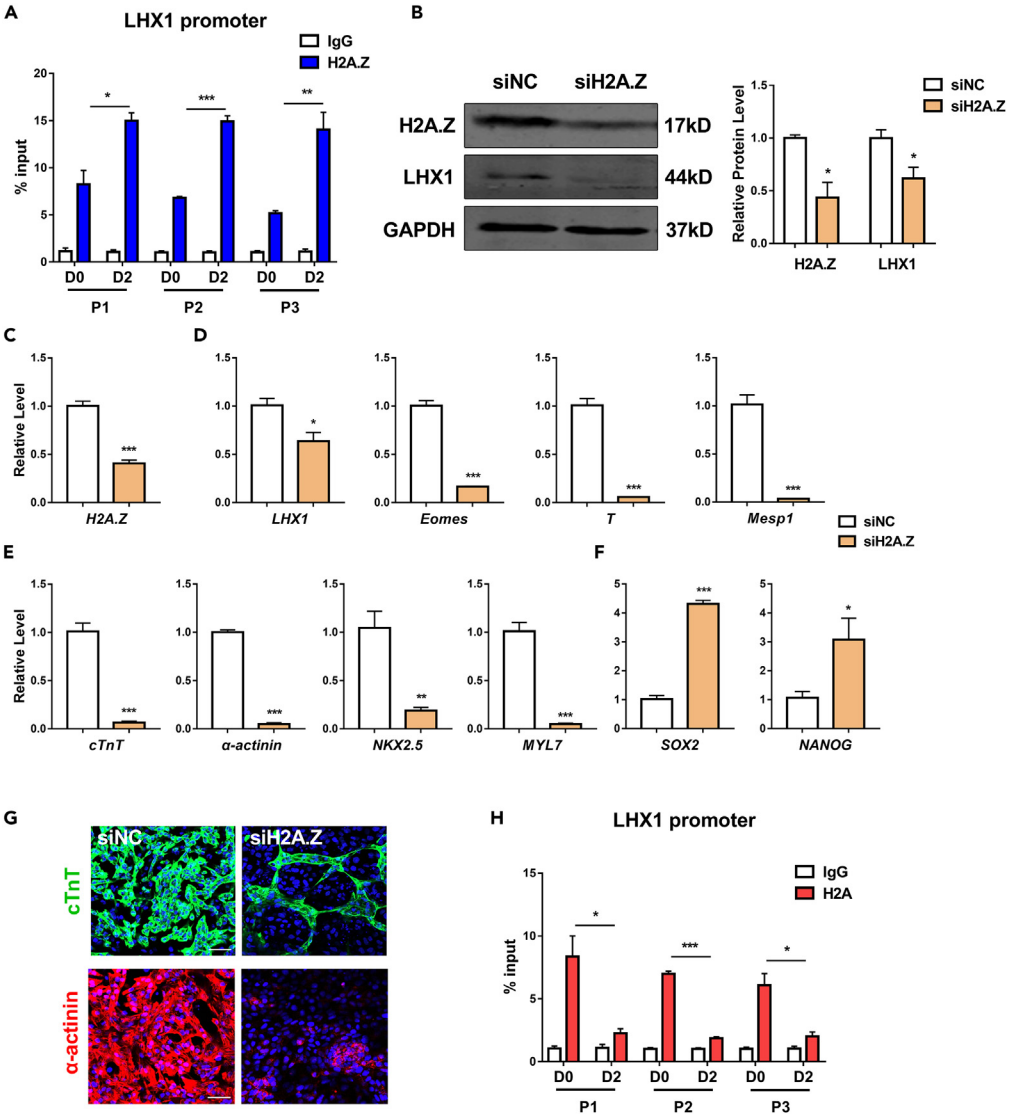

Figure 5. Histone variant H2A.Z is incorporated into the promoter of LHX1 and promotes cardiomyocyte differentiation

(A) ChIP analysis of the enrichment of H2A.Z at the promoter region of LHX1 in pluripotency and mesoderm cells. *$p < 0.05$, **$p < 0.01$, ***$p < 0.001$, n = 3.

(B) Western blot analysis of H2A.Z and LHX1 in mesoderm differentiating cells with H2A.Z knockdown. *$p < 0.05$, n = 3.

(C) qRT-PCR analysis of H2A.Z expression in differentiating hESCs 2 days following siRNA transfection of cardiac differentiation. ***$p < 0.001$, n = 4.

(D–F) qRT-PCR analysis of mesoderm markers (LHX1, Eomes, T, and Mesp1) expression on Day 2, cardiomyocyte markers (cTnT, α-actinin, NKX2.5, MYL7) expression and pluripotency markers (SOX2 and NANOG) expression on Day 10 in H2A.Z depleted hESCs. *$p < 0.05$, **$p < 0.01$, ***$p < 0.001$, n = 4.

(G) Immunostaining of cTnT (green) and α-actinin (red) in H2A.Z knockdown cells on Day 10 of CM differentiation. Scale bar, 50 μm, n = 4.

(H) ChIP analysis of the enrichment of H2A at the promoter region of LHX1 in pluripotency and mesoderm cells. *$p < 0.05$, ***$p < 0.001$, n = 3. Data are presented as mean ± SEM.

promoted LHX1 expression mainly by recruiting H2A.Z rather than regulating its expression in mesoderm. Yet, the mechanism of how *LHX1-DT* recruits H2A.Z remained unclear. Does it directly bind to H2A.Z or employ other mechanisms? To address this, we performed RNA immunoprecipitation (RIP) assay to investigate the physical binding ability between *LHX1-DT* and H2A.Z. As shown in Figure 6E, *LHX1-DT* did not specifically bind to H2A.Z. Consequently, we explored the possibility that the enrichment of H2A.Z at the LHX1 promoter region regulated by *LHX1-DT* is mediated by an intermediary protein. To investigate this, we carried out RNA pull-down assay to screen the intermediary proteins that can bind both *LHX1-DT* and H2A.Z with the sense and antisense sequences of *LHX1-DT*, respectively. Mass spectrometry (MS) identified a total of 179 proteins enriched in the sense sequence of *LHX1-DT* in MS data (Figure 6F). Immunoblotting with an anti-PHF6 antibody confirmed the binding of PHF6 to the sense sequence of *LHX1-DT* but not the antisense sequence (Figure 6G). Furthermore, it was noted that PHD finger protein 6 (PHF6) exhibited substantial enrichment and has been reported to have the potential to bind H2A.Z.[39] To investigate

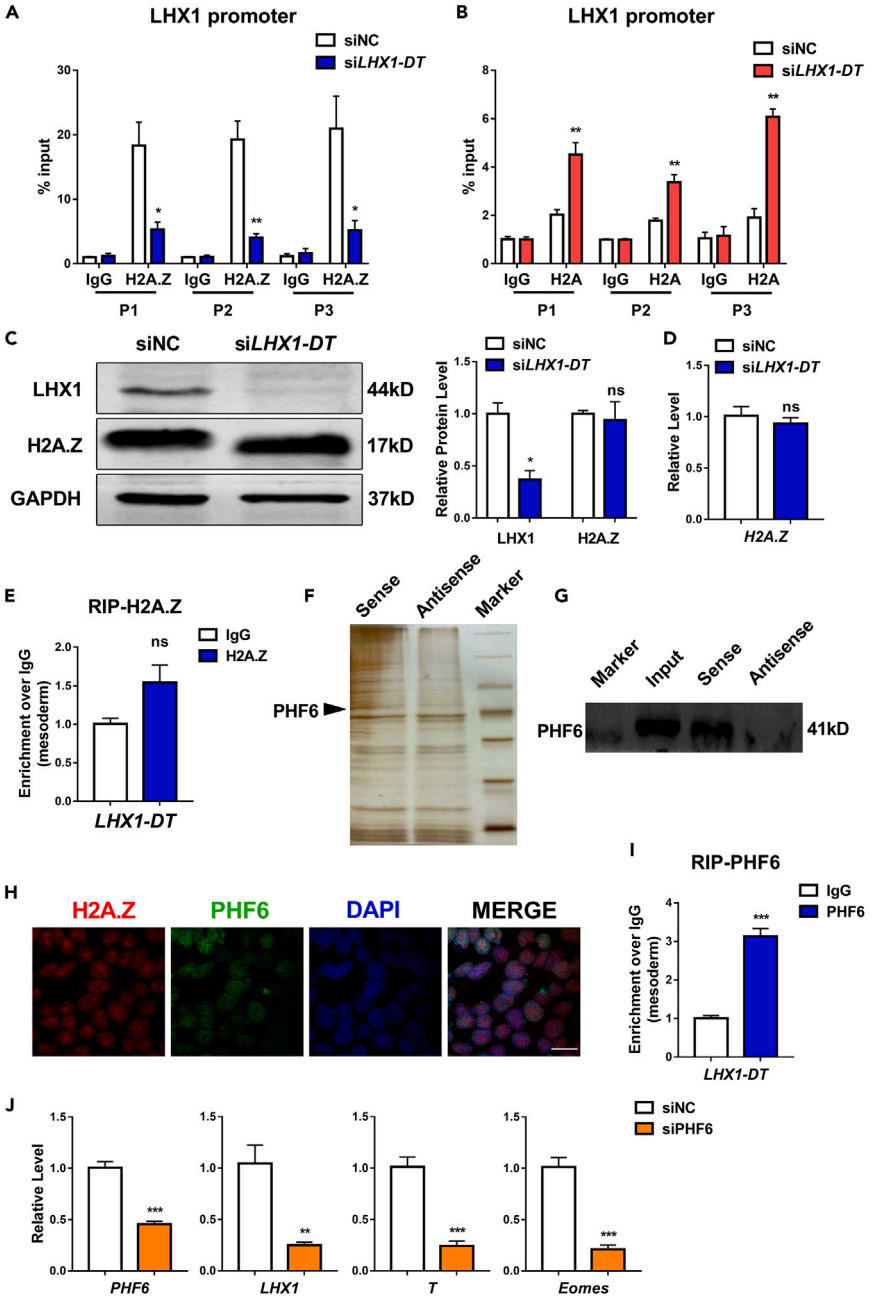

Figure 6. *LHX1-DT* promotes the replacement of H2A with H2A.Z on LHX1 promoter during mesoderm commitment

(A and B) ChIP analysis of the enrichment of H2A.Z (A) and H2A (B) at the promoter region of LHX1 upon *LHX1-DT* knockdown on Day 2. *p < 0.05, **p < 0.01, n = 3.

(C) Western blot analysis of LHX1 and H2A.Z in mesoderm differentiating cells with *LHX1-DT* knockdown. *p < 0.05, n = 3.

(D) qRT-PCR analysis of the expression level of H2A.Z on Day 2 in *LHX1-DT* depleted hESCs, n = 4.

(E) The interaction of *LHX1-DT* with H2A.Z was analyzed by an RIP assay on Day 2 of CM differentiation. n = 3.

(F) silver staining of proteins pulled down by *LHX1-DT*.

(G) Western blot analysis of PHF6 pulled down by *LHX1-DT*, n = 3.

(H) Localization of H2A.Z and PHF6 in mesodermal cells derived from hESCs by immunofluorescence assay. Scale bars, 20 μm, n = 4.

(I) The interaction of *LHX1-DT* with PHF6 was verified by an RIP assay on Day 2 of CM differentiation. ***p < 0.001, n = 3.

(J) qRT-PCR analysis of the expression levels of PHF6 and mesoderm markers (LHX1, T, and Eomes) on Day 2 in PHF6 depleted hESCs. **p < 0.01, ***p < 0.001, n = 4. Data are presented as mean ± SEM.

this further, an immunofluorescence assay was conducted, revealing co-localization of H2A.Z with PHF6, demonstrating an evidence for the binding between these two proteins. (Figure 6H). Conversely, the anti-PHF6 antibody can pull down a substantial amount of *LHX1-DT* by RIP assay (Figure 6I). Moreover, we transfected siRNA against PHF6 into hESCs to silence PHF6 expression and verified the efficiency of siPHF6, knock down of PHF6 significantly decreased the expression of mesoderm markers LHX1, T, and Eomes on Day 2 (Figure 6J). Taken together, these results indicate that *LHX1-DT* plays a critical role in modulating the enrichment of H2A.Z at the LHX1 promoter region through its interaction with the PHF6 protein. This regulatory pathway arbitrates cell fate transitions and lineage commitment during cardiac differentiation.

DISCUSSION

Cardiac differentiation is a highly intricate and rigorous process involving multiple cellular and molecular coordination. Exploring the molecular mechanism of cardiomyocyte differentiation is of great significance for elucidating the early cardiac development, evaluating drug toxicity, and advancing cell therapy. In this study, we identified a divergent lncRNA, named *LHX1-DT*, as a critical mesoderm regulator implicated in cardiogenesis.

In our previous work, we constructed a transcriptome of lncRNAs based on high-throughput sequencing datasets at four sequential stages during cardiac differentiation. We found that the relevant lncRNAs have higher similarities within each differentiation stage and higher divergence at distinct cardiac developmental stages, indicating their crucial roles at different stages of cardiac differentiation.[27] We identified a candidate lncRNA called *RP11-445F12.1*, also known as lncRNA *LHX1-DT*. *LHX1-DT* is located adjacent to the mesoendoderm marker gene LHX1 and exhibits high-expression levels during the mesoderm stage, suggesting its potential involvement in cardiac differentiation. Since *LHX1-DT* had never been investigated in the field of cardiac differentiation previously, we aimed to explore its role in depth.

Extensive evidence supports the notion that lncRNAs constitute an essential subset of the non-coding RNA family, exerting significant pathophysiological roles and various biological activities.[40] Further evidence has established the critical involvement of lncRNAs in different lineage-specific developmental processes of ESCs through diverse mechanisms.[41–43] For instance, lncRNA RCPCD impedes the differentiation of ESCs into pacemaker-like cells by inhibiting the expression of HCN4.[17] Similarly, lncRNA yylncT binds to DNMT3B, affecting DNA methylation at the T locus during mesoderm differentiation of human ESCs.[41] Additionally, lncRNA Pnky interacts with PTBP1 to control the alternative splicing of core transcript sets at the stage of neural progenitors and finally blocks neuronal development.[44] Our findings revealed a significant upregulation of *LHX1-DT* expression during the transition from embryonic stem cells to mesoderm, followed by a gradual decrease during the subsequent differentiation into cardiomyocytes. Functional studies employing a loss-of-function assay demonstrated that knock down of *LHX1-DT* significantly impaired the differentiation of hESCs into both mesoderm and cardiomyocytes. Additionally, the loss of *LHX1-DT* did not induce any discernible alterations in the typical morphology of hESCs, nor did it impact the maintenance of pluripotency. Based on these observations, we propose a hypothesis that *LHX1-DT* exerts its specific regulatory effects during the mesoderm stage, playing a pivotal role in mesoderm formation and facilitating the subsequent differentiation of hESCs into cardiomyocytes. This suggests a unique and stage-specific function of *LHX1-DT* in orchestrating the molecular events governing cardiac lineage commitment.

Approximately 20% of total lncRNAs in mammalian genomes are classified as divergent lncRNAs. Divergent lncRNAs are transcribed in the opposite direction from the promoter region of their respective neighboring protein-coding genes.[45,46] Although divergent lncRNAs are found to be correlated with tissue development in *cis*,[47] the clear functions for divergent lncRNA/mRNA gene pairs remain largely uncharacterized. In our study, we explored the co-localization and co-expression of *LHX1-DT*, as a divergent lncRNA, with its neighboring gene LHX1 during cardiomyocyte differentiation. *LHX1-DT* is localized on the human chromosome 17q12, at the vicinity of its neighboring gene LHX1 in antisense orientation. This divergent lncRNA/mRNA gene pair exhibited similar dynamic expression patterns, particularly high expression during the mesoderm stage of cardiomyocyte differentiation. LHX1 is a transcription factor that belongs to the LIM-homeodomain family; it has been proved as a mesendoderm marker.[48] It plays a critical role in the development and differentiation of various tissues and organs during embryonic development.[23,32] However, the role of LHX1 during human cardiac differentiation is still unclear. In this study, we proved that knock down of LHX1 significantly inhibited the mesoderm and cardiac differentiation. Moreover, knockdown *LHX1-DT* significantly decreased LHX1 expression, while knockdown LHX1 had no effect on *LHX1-DT* expression. On the other hand, overexpression of LHX1 rescued *LHX1-DT* depletion phenotype. These findings provide the first evidence elucidating the regulatory role of *LHX1-DT* in cardiac differentiation by controlling LHX1 transcription during mesoderm induction.

H2A.Z is one of the most conserved histone variants with 90% identity across various organisms but only shares 57% sequence identity with H2A, implying that H2A.Z has unique biological functions distinct from H2A.[49] H2A.Z has been confirmed to participate in cell fate transitions by occupying a different subset of genes in lineage-committed cells.[33] In our study, we observed a significant enrichment of H2A.Z at the promoter region of LHX1, accompanied by a decrease in H2A levels during mesoderm induction, indicating that H2A is replaced by the H2A.Z during the differentiation of hESCs into MES. Additionally, we found that knock down of endogenous H2A.Z significantly inhibited LHX1 transcription and cardiomyocyte differentiation, indicating that H2A.Z acts as an upstream regulator of LHX1. An interesting finding in the present study is that knock down of *LHX1-DT* significantly inhibited the deposition of H2A.Z to replace H2A during mesoderm induction, without affecting the expression of H2A.Z. This suggests that *LHX1-DT* regulates the deposition of H2A.Z through an indirect interaction. Furthermore, we identified PHF6, a member of plant homeodomain-like finger family, as a nuclear RNA-binding protein and histone-binding protein. The precise role of PHF6 in cardiac differentiation remained unclear until now. Previous research by Draker et al. demonstrated the specific binding of PHF6 to the histone variant H2A.Z but not to the conventional histone H2A.[39] In line with this finding, our study yielded similar results, confirming the interaction between H2A.Z and PHF6 during mesoderm induction. Consequently, our findings represent the

first experimental verification of PHF6's role as a mediator between *LHX1-DT* and H2A.Z, strengthening our understanding of the intricate regulatory mechanisms involved in cardiomyocyte differentiation.

Based on these findings, we propose a signaling pathway by which *LHX1-DT* regulates cardiomyocyte differentiation during the mesodermal stage. *LHX1-DT* exerts its regulatory function by binding to the RNA/histone-binding protein PHF6, which subsequently facilitates the recruitment of H2A.Z to the promoters of LHX1, leading to the replacement of H2A. This proposed mechanism highlights the critical role of *LHX1-DT* as a regulator in cardiomyocyte differentiation. Furthermore, aberrant regulation of mesoderm differentiation and impaired cardiac development are underlying factors in various cardiovascular disorders. By elucidating the precise mechanisms by which *LHX1-DT* influences mesoderm formation and subsequent cardiomyocyte differentiation, it may be possible to identify novel therapeutic targets for cardiac regeneration or intervention strategies for cardiovascular diseases.

Limitations of the study

In this article, our primary focus has centered on the *in vitro* validation of the regulatory role played by *LHX1-DT* in the human cardiomyocytes differentiation within the mesodermal stage. However, there exists a dearth of comprehensive understanding regarding the potential ramifications of the absence of *LHX1-DT* within the *in vivo* setting on the trajectory of cardiac development. Additionally, it is noteworthy that LHX1 serves as a pivotal regulator in the genesis of other germ layers. Thus, as the upstream of LHX1, it is plausible that the variation in the expression levels of *LHX1-DT* could wield substantial regulatory influence over the differentiation processes of distinct germ layers. Thereafter, we shall maintain a vigilant focus on the need for caveats and follow-up investigations in the realm of *in vivo* studies.

STAR★METHODS

Detailed methods are provided in the online version of this paper and include the following:

- KEY RESOURCES TABLE
- RESOURCE AVAILABILITY
  - Lead contact
  - Materials availability
  - Data and code availability
- EXPERIMENTAL MODEL AND SUBJECT DETAILS
  - Human embryonic stem cell and human induced pluripotent stem cell lines
- METHOD DETAILS
  - Cardiomyocyte differentiation
  - Bioinformatics analysis
  - Quantitative real-time polymerase chain reaction (qRT-PCR)
  - Transient transfection
  - Flow cytometry
  - RNA sequencing (RNA-Seq)
  - Knockout of *LHX1-DT* by CRISPR/Cas9
  - Immunofluorescence staining
  - Fluorescent *in situ* hybridization
  - Western blot
  - Chromatin immunoprecipitation (ChIP)
  - RNA-binding protein immunoprecipitation (RIP)
  - RNA pulldown assay
  - Mass spectrometry
- QUANTIFICATION AND STATISTICAL ANALYSIS

SUPPLEMENTAL INFORMATION

Supplemental information can be found online at https://doi.org/10.1016/j.isci.2023.108051.

ACKNOWLEDGMENTS

This work was supported by the National Natural Science Foundation of China (81970320, 82273919, 82270273 and U21A20339), CAMS Innovation Fund for Medical Sciences (CIFMS) 2019-I2M-5-078.

AUTHOR CONTRIBUTIONS

B.Y. and Y.Z. delineated the overarching research objectives. Q.Y., D.L., X.Z., M.G., X.Y., Y.W., and H.L. performed experiments and collected data. B.C., Y.Z., J.X., Z.H., Y.M., L,J, Y.B., F.Y., and L.X. provided essential study materials, reagents, instrumentation, and analysis tools. Q.Y.

CellPress
OPEN ACCESS

and Y.Z. wrote the initial draft of the manuscript. H.W. and L.S. conducted a thorough critical review of the manuscript, offering valuable commentary and insights.

DECLARATION OF INTERESTS

None declared.

Received: February 7, 2023
Revised: June 22, 2023
Accepted: September 22, 2023
Published: September 25, 2023

REFERENCES

1. Mozaffarian, D., Benjamin, E.J., Go, A.S., Arnett, D.K., Blaha, M.J., Cushman, M., de Ferranti, S., Després, J.P., Fullerton, H.J., Howard, V.J., et al. (2015). Heart disease and stroke statistics–2015 update: a report from the American Heart Association. Circulation *131*, e29–e322. https://doi.org/10.1161/CIR.0000000000000152.
2. Laflamme, M.A., and Murry, C.E. (2011). Heart regeneration. Nature *473*, 326–335. https://doi.org/10.1038/nature10147.
3. Liu, Y.W., Chen, B., Yang, X., Fugate, J.A., Kalucki, F.A., Futakuchi-Tsuchida, A., Couture, L., Vogel, K.W., Astley, C.A., Baldessari, A., et al. (2018). Human embryonic stem cell-derived cardiomyocytes restore function in infarcted hearts of non-human primates. Nat. Biotechnol. *36*, 597–605. https://doi.org/10.1038/nbt.4162.
4. Thomson, J.A., Itskovitz-Eldor, J., Shapiro, S.S., Waknitz, M.A., Swiergiel, J.J., Marshall, V.S., and Jones, J.M. (1998). Embryonic stem cell lines derived from human blastocysts. Science *282*, 1145–1147. https://doi.org/10.1126/science.282.5391.1145.
5. Kattman, S.J., Adler, E.D., and Keller, G.M. (2007). Specification of multipotential cardiovascular progenitor cells during embryonic stem cell differentiation and embryonic development. Trends Cardiovasc. Med. *17*, 240–246. https://doi.org/10.1016/j.tcm.2007.08.004.
6. Parrotta, E.I., Lucchino, V., Scaramuzzino, L., Scalise, S., and Cuda, G. (2020). Modeling Cardiac Disease Mechanisms Using Induced Pluripotent Stem Cell-Derived Cardiomyocytes: Progress, Promises and Challenges. Int. J. Mol. Sci. *21*, 4354. https://doi.org/10.3390/ijms21124354.
7. Burridge, P.W., Matsa, E., Shukla, P., Lin, Z.C., Churko, J.M., Ebert, A.D., Lan, F., Diecke, S., Huber, B., Mordwinkin, N.M., et al. (2014). Chemically defined generation of human cardiomyocytes. Nat. Methods *11*, 855–860. https://doi.org/10.1038/nmeth.2999.
8. Meilhac, S.M., and Buckingham, M.E. (2018). The deployment of cell lineages that form the mammalian heart. Nat. Rev. Cardiol. *15*, 705–724. https://doi.org/10.1038/s41569-018-0086-9.
9. Bridges, M.C., Daulagala, A.C., and Kourtidis, A. (2021). LNCcation: lncRNA localization and function. J. Cell Biol. *220*, e202009045. https://doi.org/10.1083/jcb.202009045.
10. Jiang, S., Cheng, S.J., Ren, L.C., Wang, Q., Kang, Y.J., Ding, Y., Hou, M., Yang, X.X., Lin, Y., Liang, N., and Gao, G. (2019). An expanded landscape of human long noncoding RNA. Nucleic Acids Res. *47*, 7842–7856. https://doi.org/10.1093/nar/gkz621.
11. Ulitsky, I., Shkumatava, A., Jan, C.H., Sive, H., and Bartel, D.P. (2011). Conserved function of lincRNAs in vertebrate embryonic development despite rapid sequence evolution. Cell *147*, 1537–1550. https://doi.org/10.1016/j.cell.2011.11.055.
12. Shen, B., Li, Y., Ye, Q., and Qin, Y. (2021). YY1-mediated long non-coding RNA Kcnq1ot1 promotes the tumor progression by regulating PTEN via DNMT1 in triple negative breast cancer. Cancer Gene Ther. *28*, 1099–1112. https://doi.org/10.1038/s41417-020-00254-9.
13. Boque-Sastre, R., and Guil, S. (2020). A lncRNA Decoy Predicts Sensitivity to Cisplatin. Trends Mol. Med. *26*, 352–354. https://doi.org/10.1016/j.molmed.2020.01.015.
14. Wang, W.T., Chen, T.Q., Zeng, Z.C., Pan, Q., Huang, W., Han, C., Fang, K., Sun, L.Y., Yang, Q.Q., Wang, D., et al. (2020). The lncRNA LAMP5-AS1 drives leukemia cell stemness by directly modulating DOT1L methyltransferase activity in MLL leukemia. J. Hematol. Oncol. *13*, 78. https://doi.org/10.1186/s13045-020-00909-y.
15. Andric, V., Nevers, A., Hazra, D., Auxilien, S., Menant, A., Graille, M., Palancade, B., and Rougemaille, M. (2021). A scaffold lncRNA shapes the mitosis to meiosis switch. Nat. Commun. *12*, 770. https://doi.org/10.1038/s41467-021-21032-7.
16. Ransohoff, J.D., Wei, Y., and Khavari, P.A. (2018). The functions and unique features of long intergenic non-coding RNA. Nat. Rev. Mol. Cell Biol. *19*, 143–157. https://doi.org/10.1038/nrm.2017.104.
17. Zhu, Y., You, J., Wei, W., Gu, J., Xu, C., and Gu, X. (2021). Downregulated lncRNA RCPCD promotes differentiation of embryonic stem cells into cardiac pacemaker-like cells by suppressing HCN4 promoter methylation. Cell Death Dis. *12*, 667. https://doi.org/10.1038/s41419-021-03949-5.
18. Cui, Y., Yin, Y., Xiao, Z., Zhao, Y., Chen, B., Yang, B., Xu, B., Song, H., Zou, Y., Ma, X., and Dai, J. (2019). LncRNA Neat1 mediates miR-124-induced activation of Wnt/beta-catenin signaling in spinal cord neural progenitor cells. Stem Cell Res. Ther. *10*, 400. https://doi.org/10.1186/s13287-019-1487-3.
19. Klattenhoff, C.A., Scheuermann, J.C., Surface, L.E., Bradley, R.K., Fields, P.A., Steinhauser, M.L., Ding, H., Butty, V.L., Torrey, L., Haas, S., et al. (2013). Braveheart, a long noncoding RNA required for cardiovascular lineage commitment. Cell *152*, 570–583. https://doi.org/10.1016/j.cell.2013.01.003.
20. Guo, X., Xu, Y., Wang, Z., Wu, Y., Chen, J., Wang, G., Lu, C., Jia, W., Xi, J., Zhu, S., et al. (2018). A Linc1405/Eomes Complex Promotes Cardiac Mesoderm Specification and Cardiogenesis. Cell Stem Cell *22*, 893–908.e6. https://doi.org/10.1016/j.stem.2018.04.013.
21. Li, A., Ponten, F., and dos Remedios, C.G. (2012). The interactome of LIM domain proteins: the contributions of LIM domain proteins to heart failure and heart development. Proteomics *12*, 203–225. https://doi.org/10.1002/pmic.201100492.
22. Costello, I., Nowotschin, S., Sun, X., Mould, A.W., Hadjantonakis, A.K., Bikoff, E.K., and Robertson, E.J. (2015). Lhx1 functions together with Otx2, Foxa2, and Ldb1 to govern anterior mesendoderm, node, and midline development. Genes Dev. *29*, 2108–2122. https://doi.org/10.1101/gad.268979.115.
23. McMahon, R., Sibbritt, T., Salehin, N., Osteil, P., and Tam, P.P.L. (2019). Mechanistic insights from the LHX1-driven molecular network in building the embryonic head. Dev. Growth Differ. *61*, 327–336. https://doi.org/10.1111/dgd.12609.
24. Chakraborty, D., Paszkowski-Rogacz, M., Berger, N., Ding, L., Mircetic, J., Fu, J., Iesmantavicius, V., Choudhary, C., Anastassiadis, K., Stewart, A.F., and Buchholz, F. (2017). lncRNA Panct1 Maintains Mouse Embryonic Stem Cell Identity by Regulating TOBF1 Recruitment to Oct-Sox Sequences in Early G1. Cell Rep. *21*, 3012–3021. https://doi.org/10.1016/j.celrep.2017.11.045.
25. Liu, J., Li, Y., Lin, B., Sheng, Y., and Yang, L. (2017). HBL1 Is a Human Long Noncoding RNA that Modulates Cardiomyocyte Development from Pluripotent Stem Cells by Counteracting MIR1. Dev. Cell *43*, 372. https://doi.org/10.1016/j.devcel.2017.10.026.
26. Han, Z., Xu, Z., Yu, Y., Cao, Y., Bao, Z., Gao, X., Ye, D., Yan, G., Gong, R., Xu, J., et al. (2021). ALKBH5-mediated m(6)A mRNA methylation governs human embryonic stem cell cardiac commitment. Mol. Ther. Nucleic Acids *26*, 22–33. https://doi.org/10.1016/j.omtn.2021.05.019.
27. Li, Y., Zhang, J., Huo, C., Ding, N., Li, J., Xiao, J., Lin, X., Cai, B., Zhang, Y., and Xu, J. (2017). Dynamic Organization of lncRNA and Circular RNA Regulators Collectively Controlled Cardiac Differentiation in Humans. EBioMedicine *24*, 137–146. https://doi.org/10.1016/j.ebiom.2017.09.015.
28. Wang, L., Park, H.J., Dasari, S., Wang, S., Kocher, J.P., and Li, W. (2013). CPAT: Coding-Potential Assessment Tool using an

alignment-free logistic regression model. Nucleic Acids Res. *41*, e74. https://doi.org/10.1093/nar/gkt006.
29. Kang, Y.J., Yang, D.C., Kong, L., Hou, M., Meng, Y.Q., Wei, L., and Gao, G. (2017). CPC2: a fast and accurate coding potential calculator based on sequence intrinsic features. Nucleic Acids Res. *45*, W12–W16. https://doi.org/10.1093/nar/gkx428.
30. Lin, M.F., Jungreis, I., and Kellis, M. (2011). PhyloCSF: a comparative genomics method to distinguish protein coding and non-coding regions. Bioinformatics *27*, i275–i282. https://doi.org/10.1093/bioinformatics/btr209.
31. Wang, Z., Cui, Y., Shan, Y., Kang, B., Shi, L., Geng, K., and Han, J. (2020). Generation of a MCPH1 knockout human embryonic stem cell line by CRISPR/Cas9 technology. Stem Cell Res. *49*, 102105. https://doi.org/10.1016/j.scr.2020.102105.
32. Ip, C.K., Fossat, N., Jones, V., Lamonerie, T., and Tam, P.P.L. (2014). Head formation: OTX2 regulates Dkk1 and Lhx1 activity in the anterior mesendoderm. Development *141*, 3859–3867. https://doi.org/10.1242/dev.114900.
33. Creyghton, M.P., Markoulaki, S., Levine, S.S., Hanna, J., Lodato, M.A., Sha, K., Young, R.A., Jaenisch, R., and Boyer, L.A. (2008). H2AZ is enriched at polycomb complex target genes in ES cells and is necessary for lineage commitment. Cell *135*, 649–661. https://doi.org/10.1016/j.cell.2008.09.056.
34. Faast, R., Thonglairoam, V., Schulz, T.C., Beall, J., Wells, J.R., Taylor, H., Matthaei, K., Rathjen, P.D., Tremethick, D.J., and Lyons, I. (2001). Histone variant H2A.Z is required for early mammalian development. Curr. Biol. *11*, 1183–1187. https://doi.org/10.1016/s0960-9822(01)00329-3.
35. Barski, A., Cuddapah, S., Cui, K., Roh, T.Y., Schones, D.E., Wang, Z., Wei, G., Chepelev, I., and Zhao, K. (2007). High-resolution profiling of histone methylations in the human genome. Cell *129*, 823–837. https://doi.org/10.1016/j.cell.2007.05.009.
36. Bruce, K., Myers, F.A., Mantouvalou, E., Lefevre, P., Greaves, I., Bonifer, C., Tremethick, D.J., Thorne, A.W., and Crane-Robinson, C. (2005). The replacement histone H2A.Z in a hyperacetylated form is a feature of active genes in the chicken. Nucleic Acids Res. *33*, 5633–5639. https://doi.org/10.1093/nar/gki874.
37. Chen, P., Wang, Y., and Li, G. (2014). Dynamics of histone variant H3.3 and its coregulation with H2A.Z at enhancers and promoters. Nucleus *5*, 21–27. https://doi.org/10.4161/nucl.28067.
38. Scacchetti, A., and Becker, P.B. (2021). Variation on a theme: Evolutionary strategies for H2A.Z exchange by SWR1-type remodelers. Curr. Opin. Cell Biol. *70*, 1–9. https://doi.org/10.1016/j.ceb.2020.10.014.
39. Draker, R., Ng, M.K., Sarcinella, E., Ignatchenko, V., Kislinger, T., and Cheung, P. (2012). A combination of H2A.Z and H4 acetylation recruits Brd2 to chromatin during transcriptional activation. PLoS Genet. *8*, e1003047. https://doi.org/10.1371/journal.pgen.1003047.
40. Li, M., Jiao, L., Shao, Y., Li, H., Sun, L., Yu, Q., Gong, M., Liu, D., Wang, Y., Xuan, L., et al. (2022). LncRNA-ZFAS1 Promotes Myocardial Ischemia-Reperfusion Injury Through DNA Methylation-Mediated Notch1 Down-Regulation in Mice. JACC. Basic Transl. Sci. *7*, 880–895. https://doi.org/10.1016/j.jacbts.2022.06.004.
41. Frank, S., Ahuja, G., Bartsch, D., Russ, N., Yao, W., Kuo, J.C.C., Derks, J.P., Akhade, V.S., Kargapolova, Y., Georgomanolis, T., et al. (2019). yylncT Defines a Class of Divergently Transcribed lncRNAs and Safeguards the T-mediated Mesodermal Commitment of Human PSCs. Cell Stem Cell *24*, 318–327.e8. https://doi.org/10.1016/j.stem.2018.11.005.
42. Li, C.X., Li, H.G., Huang, L.T., Kong, Y.W., Chen, F.Y., Liang, J.Y., Yu, H., and Yao, Z.R. (2017). H19 lncRNA regulates keratinocyte differentiation by targeting miR-130b-3p. Cell Death Dis. *8*, e3174. https://doi.org/10.1038/cddis.2017.516.
43. Pandey, G.K., Mitra, S., Subhash, S., Hertwig, F., Kanduri, M., Mishra, K., Fransson, S., Ganeshram, A., Mondal, T., Bandaru, S., et al. (2014). The risk-associated long noncoding RNA NBAT-1 controls neuroblastoma progression by regulating cell proliferation and neuronal differentiation. Cancer Cell *26*, 722–737. https://doi.org/10.1016/j.ccell.2014.09.014.
44. Ramos, A.D., Andersen, R.E., Liu, S.J., Nowakowski, T.J., Hong, S.J., Gertz, C., Salinas, R.D., Zarabi, H., Kriegstein, A.R., and Lim, D.A. (2015). The long noncoding RNA Pnky regulates neuronal differentiation of embryonic and postnatal neural stem cells. Cell Stem Cell *16*, 439–447. https://doi.org/10.1016/j.stem.2015.02.007.
45. Luo, S., Lu, J.Y., Liu, L., Yin, Y., Chen, C., Han, X., Wu, B., Xu, R., Liu, W., Yan, P., et al. (2016). Divergent lncRNAs Regulate Gene Expression and Lineage Differentiation in Pluripotent Cells. Cell Stem Cell *18*, 637–652. https://doi.org/10.1016/j.stem.2016.01.024.
46. Core, L.J., Waterfall, J.J., and Lis, J.T. (2008). Nascent RNA sequencing reveals widespread pausing and divergent initiation at human promoters. Science *322*, 1845–1848. https://doi.org/10.1126/science.1162228.
47. Lepoivre, C., Belhocine, M., Bergon, A., Griffon, A., Yammine, M., Vanhille, L., Zacarias-Cabeza, J., Garibal, M.A., Koch, F., Maqbool, M.A., et al. (2013). Divergent transcription is associated with promoters of transcriptional regulators. BMC Genom. *14*, 914. https://doi.org/10.1186/1471-2164-14-914.
48. Bai, H.J., Zhang, P., Ma, L., Liang, H., Wei, G., and Yang, H.T. (2019). SMYD2 Drives Mesendodermal Differentiation of Human Embryonic Stem Cells Through Mediating the Transcriptional Activation of Key Mesendodermal Genes. Stem Cell. *37*, 1401–1415. https://doi.org/10.1002/stem.3068.
49. Iouzalen, N., Moreau, J., and Méchali, M. (1996). H2A.ZI, a new variant histone expressed during Xenopus early development exhibits several distinct features from the core histone H2A. Nucleic Acids Res. *24*, 3947–3952. https://doi.org/10.1093/nar/24.20.3947.
50. Bertero, A., Fields, P.A., Ramani, V., Bonora, G., Yardimci, G.G., Reinecke, H., Pabon, L., Noble, W.S., Shendure, J., and Murry, C.E. (2019). Dynamics of genome reorganization during human cardiogenesis reveal an RBM20-dependent splicing factory. Nat. Commun. *10*, 1538. https://doi.org/10.1038/s41467-019-09483-5.
51. Szabo, L., Morey, R., Palpant, N.J., Wang, P.L., Afari, N., Jiang, C., Parast, M.M., Murry, C.E., Laurent, L.C., and Salzman, J. (2015). Statistically based splicing detection reveals neural enrichment and tissue-specific induction of circular RNA during human fetal development. Genome Biol. *16*, 126. https://doi.org/10.1186/s13059-015-0690-5.
52. Li, H., and Durbin, R. (2009). Fast and accurate short read alignment with Burrows-Wheeler transform. Bioinformatics *25*, 1754–1760. https://doi.org/10.1093/bioinformatics/btp324.
53. Trapnell, C., Roberts, A., Goff, L., Pertea, G., Kim, D., Kelley, D.R., Pimentel, H., Salzberg, S.L., Rinn, J.L., and Pachter, L. (2012). Differential gene and transcript expression analysis of RNA-seq experiments with TopHat and Cufflinks. Nat. Protoc. *7*, 562–578. https://doi.org/10.1038/nprot.2012.016.
54. Zhang, Y., Liu, T., Meyer, C.A., Eeckhoute, J., Johnson, D.S., Bernstein, B.E., Nusbaum, C., Myers, R.M., Brown, M., Li, W., and Liu, X.S. (2008). Model-based analysis of ChIP-Seq (MACS). Genome Biol. *9*, R137. https://doi.org/10.1186/gb-2008-9-9-r137.
55. Zhang, Y., Jiao, L., Sun, L., Li, Y., Gao, Y., Xu, C., Shao, Y., Li, M., Li, C., Lu, Y., et al. (2018). LncRNA ZFAS1 as a SERCA2a Inhibitor to Cause Intracellular Ca(2+) Overload and Contractile Dysfunction in a Mouse Model of Myocardial Infarction. Circ. Res. *122*, 1354–1368. https://doi.org/10.1161/CIRCRESAHA.117.312117.
56. Zhang, Y., Zhang, X., Cai, B., Li, Y., Jiang, Y., Fu, X., Zhao, Y., Gao, H., Yang, Y., Yang, J., et al. (2021). The long noncoding RNA lncCIRBIL disrupts the nuclear translocation of Bclaf1 alleviating cardiac ischemia-reperfusion injury. Nat. Commun. *12*, 522. https://doi.org/10.1038/s41467-020-20844-3.

CellPress
OPEN ACCESS

STAR★METHODS

KEY RESOURCES TABLE

REAGENT or RESOURCE	SOURCE	IDENTIFIER
Antibodies		
Monoclonal anti-cTnT	Miltenyi Biotec	Cat# 130-120-543; RRID: AB_2783888
Mouse monoclonal anti-OCT4	Santa Cruz Biotechnology	Cat# sc-5279; RRID:AB_628051
Mouse monoclonal anti-SOX2	Santa Cruz Biotechnology	Cat# sc-365823; RRID:AB_10842165
Mouse monoclonal anti-cTnT	Abcam	Cat# ab8295; RRID:AB_306445
Mouse monoclonal anti-α-actinin	Abcam	Cat# ab9465; RRID:AB_307264
Rabbit polyclonal anti-LHX1	Affinity Biosciences	Cat# DF4823; RRID:AB_2837188
Rabbit monoclonal anti-H2A.Z	Cell Signaling Technology	Cat# 50722; RRID:AB_2799379
Rabbit monoclonal anti-H2A	Cell Signaling Technology	Cat# 12349; RRID:AB_2687875
Rabbit monoclonal anti-PHF6	Abcam	Cat# ab173304
Mouse monoclonal anti-PHF6	Santa Cruz Biotechnology	Cat# sc-365237; RRID:AB_10847684
Mouse monoclonal anti-GAPDH	OriGene	Cat# TA802519; RRID: AB_2626378
Chemicals, peptides, and recombinant proteins		
Matrigel	Corning	Cat# 354277
mTeSR1	Stem Cell Technologies	Cat# 85850
CHIR99021	MedChemExpress	Cat# HY-10182
RPMI 1640	Thermo Fisher Scientific	Cat# 22400105
B27-Insulin	Thermo Fisher Scientific	Cat# A1895601
Wnt-C59	MedChemExpress	Cat# HY-15659
B27	Thermo Fisher Scientific	Cat# 17504044
TRIzol	Thermo Fisher Scientific	Cat# 15596018
SYBR Green	Roche	Cat# 04913914001
Lipofectamine RNAiMAX	Thermo Fisher Scientific	Cat# 13778150
Opti-MEM	Thermo Fisher Scientific	Cat# 31985062
ViaFect Transfection Reagent	Promega	Cat# E4982
Accutase	Sigma-Aldrich	Cat# A6964
Y-27632	MedChemExpress	Y-27632
DAPI	Roche	Cat# 10236276001
RIPA buffer	Sularbio	Cat# r0010
Protease inhibitor	Shennengbocai	Cat# P1003
Biotin	Merck	Cat# 11685597910
RNase-free DNase I	Thermo Fisher Scientific	Cat# 10777019
Streptavidin Magnetic Beads	Merck	Cat# 65001
Critical commercial assays		
Reverse Transcription Kit	TransGen Biotech	Cat# AT301-02
Fluorescent In Situ Hybridization Kit	RiboBio	Cat# C10910
ChIP assay kit	Cell Signaling Technology	Cat# 9003
RIP assay kit	Millipore	Cat# 17-701
QIA quick Gel Extraction Kit	QIAGEN	Cat# 28704

(*Continued on next page*)

Continued

REAGENT or RESOURCE	SOURCE	IDENTIFIER
Deposited data		
The RNA-seq data	This paper	Accession number:PRJNA1011895
Experimental models: Cell lines		
Human ESCs	Cellapy	H9
Human iPSCs	Cellapy	AC
Software and algorithms		
Prism	Graphpad	www.graphpad.com/scientifific-software/prism/
ImageJ	NIH	https://ImageJ.nih.gov/ij/
MACS2	Partek Flow	www.partek.com/partek-flow/

RESOURCE AVAILABILITY

Lead contact

Further information and requests for resources and reagents should be directly to and will be fulfilled by the Lead Contact, Ying Zhang (jennying223@126.com).

Materials availability

This study did not generate new unique reagents. Materials generated in this study are available from the lead contact upon request.

Data and code availability

- All data reported in this paper will be shared by the lead contact upon request.
- This paper does not report original code.
- RNA sequencing data: The RNA-sequencing data for in this paper has been deposited in NCBI Bioproject database under the accession number PRJNA1011895, BioSample accessions: SAMN37230718, SAMN37230719.

EXPERIMENTAL MODEL AND SUBJECT DETAILS

Human embryonic stem cell and human induced pluripotent stem cell lines

The validated hESC line H9 and iPSC line AC were purchased from Cellapy Biotechnology Co, China. hESCs (H9-ESCs) and hiPSCs (AC-iPSCs) were maintained in mTeSR1 media (Cat# 85850, Stem Cell Technologies, Canada) on Matrigel-coated plates (Cat# 354277, Corning, USA) at 37°C with 5% (vol/vol) CO_2. Culture medium was changed daily, cell lines were passaged every 5-6 days using Ethylenediaminetetraacetic acid (EDTA; Cat# CA3001500, Cellapy, China) and Y-27632 (Cat# HY-10071, MCE, USA). Cultures were maintained in an undifferentiated state at 37°C and 5% CO_2.

METHOD DETAILS

Cardiomyocyte differentiation

For cardiomyocyte differentiation, stem cells (80%–90% confluence) were treated with 6 μM CHIR99021 (Cat# HY-10182, MCE, USA) in RPMI 1640 (Cat# 22400105, Thermo Fisher Scientific, USA) and B27 supplement minus insulin (Cat# A1895601, Thermo Fisher Scientific, USA) (RPMI+B27-Insulin) for 2 days. On day 2 (D2), cells were placed in RPMI+B27-Insulin without CHIR99021. On days 3-4, cells were treated with 2 μM Wnt-C59 (Cat# HY-15659, MCE, USA) in RPMI+B27-Insulin. On days 5-6, cells were placed in RPMI+B27-Insulin without Wnt-C59. From day 7, cells were cultured in RPMI and B27 supplement (Cat# 17504044, Thermo Fisher Scientific, USA) (RPMI+B27+Insulin). The medium was changed every 48 h until beating was observed.

Bioinformatics analysis

We obtained transcriptomic and epigenomic data in four different stages of human cardiac differentiation via the SRA Toolkit from the SRA database (GSE106690, GSE64417), including embryonic stem cells (D0), mesoderm (D2), cardiac progenitor (D5) and cardiomyocytes (D10) in RUES2 hESC lines, respectively.[50,51] The reads were aligned to hg38 genome using tophat for RNA-Seq and BWA (Version: 0.7.12)[52] for ATAC-Seq. CuffLinks[53] was further used to calculate RNA expression levels. For ATAC-Seq data, peak calling was used MACS2 to analyze.[54] The specific expression of genes in the MES stage was defined as those with significantly high expression levels at this stage. Differentially expressed analyses were realized by Cuffdiff (FDR<0.01).[53] Then, the intersect genes were used for further co-expression network construction and functional analysis. The co-expression network was created by Spearman's correlation (R>=0.6; FDR<0.1) among specific expression genes at the MES stage, including *LHX1-DT* and LHX1. Functional analysis was performed by clusterProfiler (adjusted P<0.1).

Quantitative real-time polymerase chain reaction (qRT-PCR)

We collected the cells at different time points (Day 0, Day 2, Day 5 and Day 10) during the process of cardiac differentiation. Total RNA extraction and qRT-PCR were performed as described previously.[55] Total RNA was extracted by TRIzol (Cat# 15596018, Thermo Fisher Scientific, USA) according to the manufacturer's instructions. The concentration and the quality of RNA were measured by NanoDrop-8000 spectrophotometer (Cat# ND-8000-GL, Thermo Fisher Scientific, USA). Total RNA was reversely transcribed to cDNA with a Reverse Transcription Kit (Cat# AT301-02, TransGen Biotech, China). Then cDNA was amplified with SYBR Green (Cat# 04913914001, Roche, Switzerland) and measured by 7,500 Real Time-PCR System (Applied Biosystems, USA). The relative quantitative expression was calculated according to the $2^{-\Delta\Delta CT}$ method. The primer sequences used in this study are listed in Table S1.

Transient transfection

We transfected small interfering RNA (siRNA) to silence *LHX1-DT* (si*LHX1-DT*), LHX1 (siLHX1) and H2A.Z (siH2A.Z) into differentiating hESCs. The transfection was performed with 6 μL of Lipofectamine RNAiMAX Reagent (Cat# 13778150, Thermo Fisher Scientific, USA) and 100 nM of siRNA in 200 μL Opti-Minimal Essential Medium (Opti-MEM, Cat# 31985062, Thermo Fisher Scientific, USA) together and incubated in 12-well plates at room temperature (RT) for 5 min when cells reached 70%–80% confluence. The sequence of siRNA was listed in Table S2. 2 μg LHX1-overexpressed plasmid and 8 μL ViaFect Transfection Reagent (Cat# E4982, Promega, USA) were diluted in 200 μL Opti-MEM and stood for 20 min. Then the cells were incubated with the transfection mixture described above in 12-well plates.

Flow cytometry

Flow cytometry was performed to detect cTnT-positive cardiomyocytes on differentiation Day 10. Briefly, cells were dissociated with Accutase (Cat# A6964, Sigma-Aldrich, USA) at 37°C for 2 min, and the digestion was terminated with RPMI+B27+Insulin. After washed with DPBS, the cells were incubated with cTnT antibody (Cat# 130-120-543, Miltenyi Biotec, Germany, 1:50) for 20 min. The samples were measured by using a Beckman Coulter flow cytometer, and the results were analyzed by using FACScan flow cytometer with Cell Quest software (Beckman Coulter, USA).

RNA sequencing (RNA-Seq)

Sequencing and cDNA library construction were performed with the NovaSeq 6000 platform (Illumina, USA). RNA integrity and gDNA contamination were confirmed by denaturing agarose gel electrophoresis, and the sequencing library was tested by an Agilent 2100 Bioanalyzer using the Agilent DNA 1000 ChIP Kit (Cat# 5067-1504, Agilent, USA). The differential expressed genes (DEGs) were identified to explore the functional enrichment analysis of Gene Ontology (GO) and Kyoto Encyclopedia of Genes and Genomes (KEGG) pathway.

Knockout of *LHX1-DT* by CRISPR/Cas9

CRISPR/Cas9-mediated genomic knockout was performed to generate *LHX1-DT*$^{-/-}$ cell lines as previously reported.[31] Guide RNAs (gRNAs) sequences were designed using the web resource http://crispr.mit.edu/. Briefly, homologous arm donor DNAs targeting gene containing left and right homology arms and a LoxP-flanked PGK-puromycin cassette were used. About 1×10^6 cells were electroporated with 2 μg of donor DNA and 4 μg of pX330 plasmid containing the Cas9 protein sequence and the corresponding gRNAs for the knockout *LHX1-DT*. Then, the electroporated cells were plated on six-well plates and selected positive clones by using Puromycin after 24 h. Positive clones were plated on 6-well plates coated with Matrigel in mTeSR1 with 10 μM Y-27632 (Cat# HY-10071, MCE, USA) for 2 days. Two *LHX1-DT*$^{-/-}$ clones were selected and confirmed by qRT-PCR.

Immunofluorescence staining

Cells were fixed with 4% Paraformaldehyde for 15 min, permeabilized with 0.1% Triton X-100 for 45 min, and blocked in 50% goat serum for 1 h at RT. The cells were subsequently stained with antibodies to OCT4 (Cat# sc-5279, Santa Cruz, USA, 1:400), SOX2 (Cat# sc-365823, Santa Cruz, USA, 1:400), cTnT (Cat# ab8295, Abcam, UK, 1:400), α-actinin (Cat# ab9465, Abcam, UK, 1:400), H2A.Z (Cat# 50722, Cell Signaling Technology, 1:1000) and PHF6 (Cat# sc-365237, Santa Cruz, USA, 1:500) separately, at 4°C overnight. The cells were washed with PBS, followed by incubation with the conjugated secondary antibody in the dark for 1 h. Nuclei were stained with DAPI (Cat# 10236276001, Roche, USA) at RT. The samples were imaged with a laser scanning confocal microscope (Zeiss, Germany).

Fluorescent *in situ* hybridization

Fluorescent in situ hybridization (FISH) was conducted with Fluorescent In Situ Hybridization Kit (Cat# C10910, RiboBio, Guangzhou, China) according to the manufacturer's instructions to determine the cellular distribution of *LHX1-DT* and LHX1. In brief, the cells were fixed with 4% paraformaldehyde for 10 min, washed three times with PBS and penetrated with 0.5% Triton X-100 at RT. Then, they were incubated with *LHX1-DT* probes at 37°C overnight, by sequential washing with Saline Sodium Citrate Buffer (SSC) at 42°C and subsequent incubation with anti-LHX1 antibody (Cat# DF4823, affinity, USA, 1:400) at 4°C overnight. Nucleus were stained with DAPI (Cat# 10236276001, Roche, USA) at RT. The samples were imaged under a laser scanning confocal microscope (Zeiss, Germany).

Western blot

Cells were harvested with RIPA buffer (Cat# r0010, Sularbio, China) containing protease inhibitor (Cat# P1003, Shennengbocai, China). The whole-cell lysates were fractionated by SDS-PAGE. Proteins were transferred to a nitrocellulose membrane, which was then incubated with the primary antibodies for anti-LHX1 (Cat# DF4823, affinity, USA, 1:1000), anti-H2A.Z (Cat# 50722, Cell Signaling Technology, USA, 1:1000), anti-OCT4 (Cat# sc-5279, Santa Cruz, USA, 1:1,000), and anti-GAPDH (Cat# TA802519, OriGene, USA, 1:1,000) at 4°C overnight. After washed with PBST for 3 times, the membrane was incubated with secondary antibody at RT for 1 h. The relative expression of protein was detected and quantified by Odyssey infrared scanning system (LI-COR, USA).

Chromatin immunoprecipitation (ChIP)

ChIP experiment was performed using SimpleChIP® Enzymatic Chromatin IP Kit (Cat# 9003, Cell Signaling Technology, USA) according to the manufacturer's instructions. Briefly, 4×10^7 mesoderm cells were cross-linked with 1% formaldehyde at RT for 10 min. The chromatin was fragmented by nuclease to obtain chromatin fragments of 1-5 nucleosomes in size. Chromatin fragments was immunoprecipitated with anti-H2A.Z antibody (Cat# 50722, Cell Signaling Technology, USA) and anti-H2A antibody (Cat# 12349, Cell Signaling Technology, USA). Purified DNA was used for quantitative PCR analyses, and the data were normalized to input chromatin. The primer pair sequences used in this study for ChIP assays are listed in Table S3.

RNA-binding protein immunoprecipitation (RIP)

RIP assay was conducted with Magna RIP™ RNA-Binding Protein Immunoprecipitation Kit (Cat# 17-701, Millipore, Germany) according to manufacturer's instructions. Briefly, the cells that from hESC-derived mesoderm were lysed with lysis buffer containing protease inhibitors and RNase Inhibitor. The cell lysates were incubated with magnetic beads conjugated with anti-H2A.Z antibody (Cat# 50722, Cell Signaling Technology, USA) and anti-PHF6 antibody (Cat# ab173304, Abcam, UK) overnight at 4°C. The coprecipitated RNAs were isolated after protein digestion with proteinase K. The purified RNAs were reversely transcribed to cDNA and subject to qRT-PCR. The enrichment was calculated relative to the percentage of input.

RNA pulldown assay

RNA pulldown assay was performed as described previously.[56] LncRNA *LHX1-DT* was subcloned into GV208 plasmid and purified with QIA quick Gel Extraction Kit (Cat# 28704, QIAGEN, Germany). The plasmid DNA was transcribed to RNA that was then labeled with biotin (Cat# 11685597910, Merck, Germany). Then, the biotinylated RNAs were treated with RNase-free DNase I (Cat# 10777019, Thermofisher scientific, USA) and using Quick Spin columns (Cat# 11274015001, Merck, Germany) to purify the biotinylated RNAs. The streptavidin magnetic beads (Cat# 65001, Merck, Germany) were added into proteins and RNAs, shaken vigorously and centrifuged, then the supernatant was discarded. The eluted RNA bound protein was then analyzed by mass spectrometry assay and Western blot analysis. The antisense of *LHX1-DT* was employed as a negative control.

Mass spectrometry

Mass spectrometry (MS) was performed by Wuhan GeneCreate Biological Engineering Co., Ltd. In briefly, samples were subjected to enzymolysis in protein gel, desalting and LC-MS/MS analysis. Then submit the original MS/MS files from the mass spectrometer to ProteinPilot for data analysis. For the identified protein results, select certain filtering criteria, and peptides with an unused score > 1.3 (a credibility of more than 95%) are considered credible peptides, and proteins containing at least one unique peptide are retained.

QUANTIFICATION AND STATISTICAL ANALYSIS

Data are shown as mean ± SEM. Each data point was obtained from at least three independent experiments. Student's t test was used for two-group comparisons, and one-way analysis of variance tests were used for multi-group comparisons. Differences with P values < 0.05 were regarded as significant. The statistical analyses were performed with the use of Prism version 8.0 software (GraphPad Software).